Understanding the Molecular Basis of Salt Sequestration in Epidermal Bladder Cells of *Chenopodium quinoa*

Highlights

- HKT1-type channels mediate a one-way sodium load into quinoa bladder cells

- ClC transporters operate in the Cl$^-$ sequestration into vacuoles of bladder cells

- The bladder cytoplasm is osmotically balanced by potassium and proline import

- On the transcript level, bladders are "constitutively active" for salt sequestration

Authors

Jennifer Böhm, Maxim Messerer,
Heike M. Müller, ..., Georg Haberer,
Jian-Kang Zhu, Rainer Hedrich

Correspondence

g.haberer@helmholtz-muenchen.de
(G.H.),
zhu132@purdue.edu (J.-K.Z.),
hedrich@botanik.uni-wuerzburg.de (R.H.)

In Brief

Böhm et al. report that the inward-rectifier CqHKT1.2 is a key player for the Na$^+$ load into bladder cells under salinity stress. Together with transporters for compatible solutes, these transport systems mediate sequestration of salt into bladders, arming quinoa with an efficient mechanism to protect the metabolically active photosynthetic tissues.

CellPress

Understanding the Molecular Basis of Salt Sequestration in Epidermal Bladder Cells of *Chenopodium quinoa*

Jennifer Böhm,[1,12] Maxim Messerer,[2,12] Heike M. Müller,[3,12] Joachim Scholz-Starke,[4] Antonella Gradogna,[4] Sönke Scherzer,[3] Tobias Maierhofer,[3] Nadia Bazihizina,[1,5] Heng Zhang,[6] Christian Stigloher,[7] Peter Ache,[3] Khaled A.S. Al-Rasheid,[8] Klaus F.X. Mayer,[2] Sergey Shabala,[1,9] Armando Carpaneto,[4,10] Georg Haberer,[2,*] Jian-Kang Zhu,[6,11,*] and Rainer Hedrich[3,13,*]

[1]Tasmanian Institute for Agriculture, College of Science and Engineering, University of Tasmania, Private Bag 54, Hobart, TAS 7001, Australia
[2]Plant Genome and Systems Biology, Helmholtz Center Munich, Ingolstädter Landstraße 1, 85764 Neuherberg, Germany
[3]Institute for Molecular Plant Physiology and Biophysics, University of Wuerzburg, Julius-von-Sachs Platz 2, 97082 Wuerzburg, Germany
[4]Institute of Biophysics, National Research Council (CNR), Via De Marini 6, 16149 Genova, Italy
[5]Department of Agrifood Production and Environmental Sciences, Università degli Studi di Firenze, Viale delle Idee 30, 50019 Sesto Fiorentino, Florence, Italy
[6]Shanghai Center for Plant Stress Biology, and CAS Center for Excellence in Molecular Plant Sciences, 3888 Chenhua Road, Shanghai 201602, China
[7]Imaging Core Facility, Biocenter, University of Wuerzburg, Am Hubland, 97074 Wuerzburg, Germany
[8]Zoology Department, College of Science, King Saud University, PO Box 2455, Riyadh 11451, Saudi Arabia
[9]Department of Horticulture, Foshan University, Foshan 528000, PRC
[10]Department of Earth, Environment and Life Sciences (DISTAV), University of Genoa, Viale Benedetto XV 5, 16132 Genoa, Italy
[11]Department of Horticulture and Landscape Architecture, Purdue University, 625 Agriculture Mall Drive, West Lafayette, IN 47907, USA
[12]These authors contributed equally
[13]Lead Contact
*Correspondence: g.haberer@helmholtz-muenchen.de (G.H.), zhu132@purdue.edu (J.-K.Z.), hedrich@botanik.uni-wuerzburg.de (R.H.)
https://doi.org/10.1016/j.cub.2018.08.004

SUMMARY

Soil salinity is destroying arable land and is considered to be one of the major threats to global food security in the 21st century. Therefore, the ability of naturally salt-tolerant halophyte plants to sequester large quantities of salt in external structures, such as epidermal bladder cells (EBCs), is of great interest. Using *Chenopodium quinoa*, a pseudo-cereal halophyte of great economic potential, we have shown previously that, upon removal of salt bladders, quinoa becomes salt sensitive. In this work, we analyzed the molecular mechanism underlying the unique salt dumping capabilities of bladder cells in quinoa. The transporters differentially expressed in the EBC transcriptome and functional electrophysiological testing of key EBC transporters in *Xenopus* oocytes revealed that loading of Na$^+$ and Cl$^-$ into EBCs is mediated by a set of tailored plasma and vacuole membrane-based sodium-selective channel and chloride-permeable transporter.

INTRODUCTION

Soil salinity is one of the major environmental factors causing crop loss worldwide. To sustain the world's food supply, salt tolerance is becoming an increasingly important agronomic trait to advance crop production on saline soils. Salinity stress of crops is associated with an increase in Na$^+$ and Cl$^-$ ions in the plant body. However, there are plants known as halophytes that can tolerate salinity. Among them are members of the *Amaranthaceae*, including quinoa (*Chenopodium quinoa*), that tolerates saline soils and episodes of soil drying [1]. To utilize the genetic resources for next-generation breeding of quinoa to improve performance and production under stressful environments, the genome of this species was sequenced very recently [2–4]. These genomic resources offer a valuable tool for answering questions about the molecular basis of salt tolerance in quinoa. When quinoa was compared to its chenopod relatives sugar beet and spinach, an expansion of genes involved in ion and nutrient transport was detected as well as a morphological difference, namely the ability of quinoa to develop epidermal bladder cells (EBCs). When quinoa is grown in saline soils, the halophyte takes up sodium and chloride ions to osmotically adapt to a decrease in water potential. To prevent young, growing leaves from salt stress disorders, Na$^+$ and Cl$^-$ are stored in the EBCs. These spherical leaf-external structures are 200 to 1,000 times larger in volume than common leaf cells, thus well suited to serve as salt dumpers. In some species, such as the classical CAM (crassulacean acid metabolism) model *Mesembryanthemum* [5–7], salt bladders can store up to 1 M NaCl, within a giant vacuole. To reach the final destination in the EBC vacuole, salt has to travel from root to leaf. At the level of the bladders, Na$^+$ and Cl$^-$ need to cross the plasma membrane (PM), pass the cytoplasm, and finally get loaded in the vacuole lumen of the salt dumper. We have recently shown that loss of EBCs results in a salt-sensitive phenotype under saline conditions [8], which
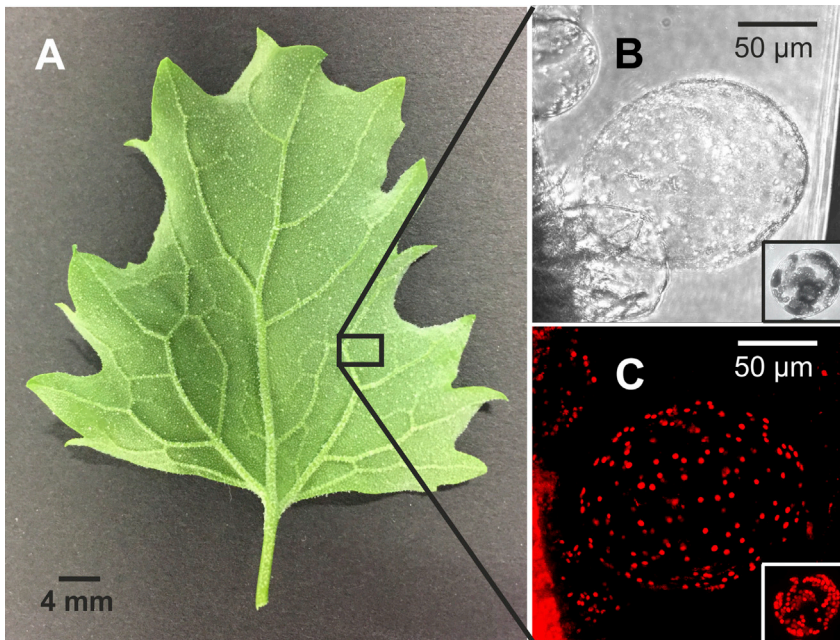
Figure 1. Lower Photosynthetic Activity in EBCs Could Be Affiliated to a Lower Density of Chloroplasts

(A) Image of a young quinoa leaf grown under control conditions.

(B) Image of a single EBC on the leaf surface and of a mesophyll protoplast (inset) under transmitted light conditions.

(C) The corresponding chlorophyll fluorescence of the single EBC and the mesophyll protoplast are shown in (C) and inset of (C), respectively.

See also Figure S1, Table S2, and Data S1.

entially expressed at a false discovery rate (FDR) $\leq$ 0.05 and 6,469 (15.8%) by a fold change $\geq$ 2 for the B/L comparison (Table S1). In response to salt, we identified 1,659 differentially expressed transcripts in non-brushed leaves (comparison: L+/L) and 1,702 in EBCs (comparison: B+/B; Table S1).
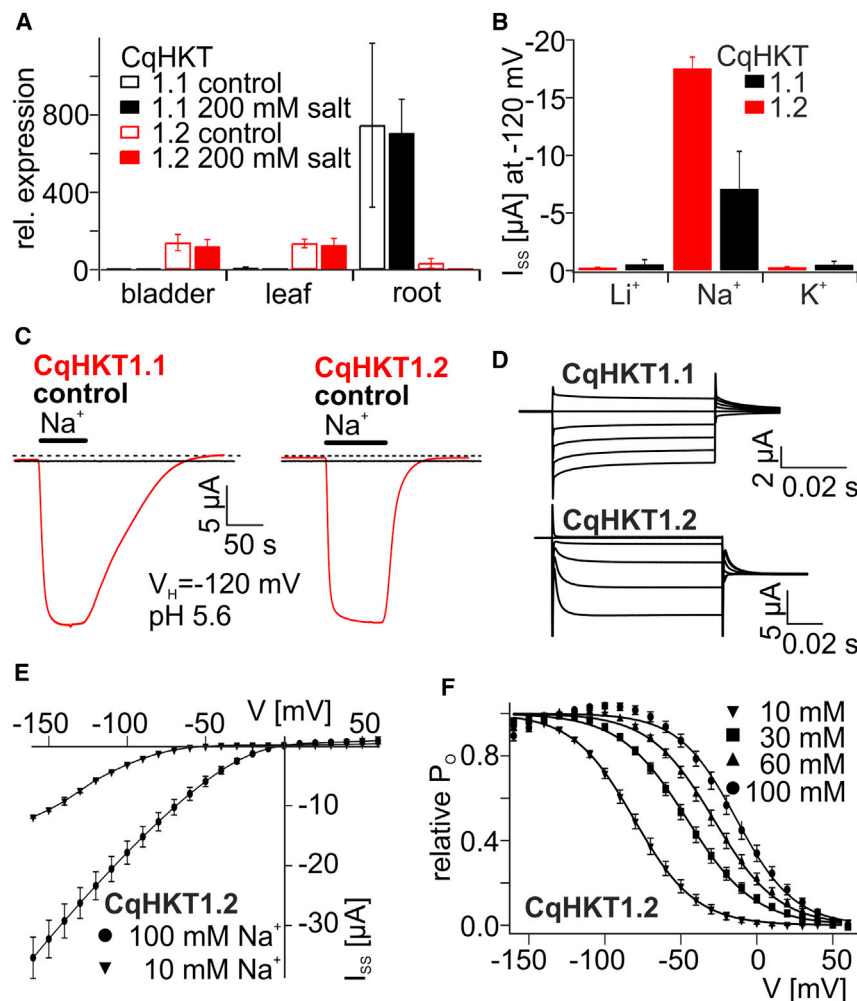
These genes work in numerous biological processes, but there are clear patterns in several housekeeping pathways affecting carbon fixation and the generation and consumption of energy with the heterotrophic bladder. Chloroplasts of EBCs appear randomly distributed along the cell, whereas mesophyll cell chloroplasts are densely packed (Figures 1A–1C). Although both cell types show an equal number of chloroplasts, the difference in cell type size resulted in an EBC chloroplast density of 2.7×10^4 per μm^3, and mesophyll cells harbor 49.8×10^4 chloroplasts per μm^3, which is 18-fold higher (Table S2). Interestingly, and in contrast to mesophyll chloroplasts, bladder chloroplasts lack grana (Figures S1A and S1B), the most prominent location of Photosystem II (PSII) [14]. It thus did not come expected that genes of the light harvesting complex and PSII were found not or just weakly expressed (Data S1A). Together, these features of bladder chloroplasts pointed to a reduced gross photosynthetic activity in EBCs (Data S1A). It is tempting to speculate that bladder chloroplasts operate cyclic electron transport and, together with the mitochondria, produce ATP to energize salt transport.

To feed the mitochondria and thus the major energy demands of the heterotrophic EBCs, sugar import into bladders is indispensable. We found the level of more than 20 out of 86 sugar transporter transcripts higher in bladders than leaves (Data S2A). In line with a minor role of bladders in carbon fixation, most genes of the pentose phosphate cycle were upregulated in leaves (Data S1B). Vice versa, energy (ATP)-producing catabolic pathways were emphasized in bladders. Genes of the citrate cycle were generally expressed at higher levels in bladders compared to leaves (Data S1C). A major source of the required acetyl-coenzyme A (CoA) likely originates from the β-oxidization of fatty acids: all genes involved in the degradation of fatty acids were expressed at significantly higher levels in EBCs (Data S1D).

could be associated with major leaf ionic and metabolic rearrangements.

Here, we investigated the molecular mechanisms that enable EBCs to handle high salt doses. EBCs are common to several halophytic plants, enabling the salinity-tolerant plants to deposit sodium and chloride into external leaf stores. Although these structures are of primary importance for bladder-growing halophytes, the molecular mechanism of how salt is directed into EBCs has remained entirely unknown. To answer this question, we analyzed high-depth transcriptome data from EBCs obtained from quinoa grown in the presence and absence of soil salinity and functionally analyzed bladder-expressed transporters.

RESULTS

Transcript profiling by RNA sequencing (RNA-seq), microarray analysis, or real-time qPCR is a well-established tool to determine the cell-type-specific expression of genes of interest and was already used for either single cell types, such as trichomes and guard cells of *Nicotiana tabacum* and *Arabidopsis* [9–12], or tissues containing several types of cells, like the glands of the Venus flytrap [13]. In this research, we focused on two RNA profiling approaches (RNA-seq and qPCR) to investigate the bladder specification and function in the context of salt stress.

Salt Bladders Are Heterotrophic in Nature

Clustering analyses showed that bladders exhibit a unique transcriptome profile consistent with EBCs being specialized for osmoregulation and salt sequestration [4]. Consistent with this specialized role of EBCs, we detected many differentially expressed genes between RNA-seq data from the two tissue types. After filtering for lowly expressed genes, we observed expression for 40,907 out of the 54,682 total genes (74.8%) present in the quinoa genome. Of these, 16,809 (41.1%) were differ-

Testing the Salt Sequestration Model

Using the tool SubaCon, we identified 586 PM and vacuole transporter genes in total (Data S2B). We found 316 PM and

Figure 2. Quinoa HKT1-like Channels: Different Localizations Require Distinct Electrophysiological Properties

(A) qPCR of two quinoa HKT1-like channels. CqHKT1.1 is only expressed in roots and is not affected by salt. CqHKT1.2 remarkably has expression levels lower than CqHKT1.1 but 4 times higher in bladders and leaves compared to roots (mean ± SE; n ≥ 7).

(B) I_{SS} in LiCl, NaCl, and KCl (100 mM each; pH 5.6) illustrate the sodium selectivity of both HKT1 channels (mean ± SD; n ≥ 4).

(C) Sodium-induced inward currents could be recorded in CqHKT1.1- and CqHKT1.2-expressing oocytes compared to control cells, when 100 mM NaCl was applied. The dotted line represents zero current.

(D) Whole-cell current responses to voltage pulses ranging from +40 mV to −160 mV in 40-mV decrements and 100 mM NaCl. Instantaneous outward and inward currents could be recorded for CqHKT1.1, whereas CqHKT1.2 exclusively revealed inward currents.

(E) CqHKT1.2-mediated sodium currents in 10 or 100 mM NaCl. The current-voltage relation of CqHKT1.2 shows inward-directed sodium currents, which increased with higher external Na+ concentrations (mean ± SD; n = 6).

(F) The relative open probability of CqHKT1.2-expressing oocytes at the indicated Na+ concentrations was plotted against the applied test voltages. Note the prominent negative shift of the half-maximal activation potential from −13 mV at 100 mM Na+ to −80 mV at 10 mM Na+ (mean ± SD; n = 5).

See also Figures S2 and S3 and Data S2.

vacuole transporter transcripts differentially expressed between brushed leaves and EBCs already under control conditions. The observed changes in the transcriptome are consistent with the role of EBCs in salt sequestration (see below).

Sodium and chloride uphill transport across the plasma and vacuole membrane of EBCs require a coupling to the electrochemical potential. Next, we performed a detailed analysis first of the expression and function of sodium and chloride transporters and second of the balancing of compatible osmolytes.

Plasma Membrane Transport

There is ample evidence that SOS1 and HKT1 systems are major players in plant Na+ transport across the PM [15, 16]. SOS1 (salt overly sensitive 1) represents a Na+/H+-antiporter that uses the proton-motive-force (PMF) to move Na+ out of the cell [17–19], thereby preventing the cytoplasm from reaching toxic levels of sodium. Interestingly, when compared to leaf, SOS1 transcripts were found at quite low levels in bladders (Data S2C). We could confirm these findings by examining expression levels of a SOS1 homolog by qPCR (Data S2D), which is consistent with bladder function in Na+ accumulation rather than export. However, we found constitutively high expression of the sodium-permeable ion channel HKT1 in bladders (Data S2C).

Vacuole Membrane Transport

We found a similar high constitutive bladder expression for NHX1 and ClC-c quinoa orthologs, which are well known as vacuolar proton-coupled Na+ and anion exchangers (Data S2C). Besides the two H+-coupled solute transporters, the transcripts of vacuolar proton pumps were also present at a higher level in the bladder than the leaf (Data S2E). The latter finding supports the notion that the PMF would drive Na+ and Cl− movement into the bladder vacuole against a progressively increasing concentration gradient (of up to 1 M) [7, 20]. We then selected the PM sodium channel CqHKT1 and the vacuolar anion transporter CqClC-c for testing EBC specific functions in detail.

Bladder Sodium Channel Possesses Unique Voltage-Dependent Properties

HKT-type channels were identified in genetic screens for salt-tolerant crops [21–23] and found to mediate Na+-selective or a combined K+/Na+ transport across the PM [16, 23]. We identified two co-orthologs of AtHKT1 in quinoa; CqHKT1.1 is predominately expressed in roots (Figure 2A), and CqHKT1.2 transcripts are found in leaves and, most importantly, in EBCs (Figure 2A). We analyzed the phylogenetic relationship between CqHKTs

and HKTs from different plant species and classified them as members of the HKT subclass 1 (Figure S2A). In line with this classification, both CqHKTs carry a serine residue in the first pore loop rather than the glycine of class II members (Figure S2B) [23, 24].

When CqHKT:mOrange constructs were each transiently expressed in *Arabidopsis* protoplasts, the fluorophore was localized at the PM (Figures S3A and S3B). For functional analysis, both CqHKTs were expressed in *Xenopus* oocytes. The bladder-expressed CqHKT1.2 shares 40.91% identity at the amino acid level and shares strict sodium selectivity with CqHKT1.1 (Figure 2B). Upon membrane hyperpolarization and the presence of sodium, CqHKT1.2 mediated inward Na^+ currents (Figure 2C). When the extracellular NaCl concentration was increased stepwise to 100 mM, the reversal potential (V_{rev}) shifted to positive voltages following the Nernst potential of Na^+ for both CqHKTs (Figure S3C). The CqHKT1.2-mediated sodium currents proceed in a linear manner under increasing external NaCl conditions and did not show saturation kinetics (c.f. CqHKT1.1; Figure S3D). Furthermore, CqHKT1.1- and 1.2-mediated currents did not change in a pH-dependent manner. This behavior shows that both CqHKTs operate as Na^+ channels rather than proton-driven transporters. Interestingly, in contrast to CqHKT1.1, the bladder CqHKT1.2 exhibited the hallmark features of a voltage-dependent, plant inward-rectifying potassium channel of the KAT type (Figure 2D). In the presence of extracellular 10 mM Na^+, CqHKT1.2 currents were activated negative to -60 mV. Upon a shift to 100 mM Na^+, the threshold of voltage activation shifted to -10 mV (Figure 2E). Also, ion flux measurements under voltage-clamp conditions documented the characteristic hyperpolarization activation of CqHKT1.2. As expected from the current-voltage curves at +60 mV, CqHKT1.1 mediated Na^+ efflux but CqHKT1.2 did not (Figure S3E). In line with the latter HKT1 isoform operating as an inward rectifier, Na^+ influx appeared at negative potentials only (Figure S3E). The activation kinetics of CqHKT1.2 could be fitted by a double exponential, revealing a fast activation constant of 2–4 ms. This activation is roughly 50 times faster than the activation that is described for the plant K^+ Shaker channel KAT1 [25].

To test whether Na^+ via CqHKT1.2 could leak out of the cell upon membrane depolarization, we analyzed channel activation as a function of voltage and Na^+ concentration (Figure 2F). Under low external sodium concentrations, CqHKT1.2 activated at more negative voltages. This behavior indicates that CqHKT1.2 prevents sodium leakage from the EBCs even under low external sodium concentration, resulting in steep outward-directed sodium gradients. Interestingly, the bladders from the halophytic CAM plant *Mesembryanthemum crystallinum* express a CqHKT1.1- and CqHKT1.2-type moiety [23]. The McHKT1.2 (AAK52962.1) also mediates a voltage-dependent sodium influx (Figures S3F and S3G) and therefore shows the same rectifying characteristics as CqHKT1.2. Together, the features of both bladder HKTs document that, in the presence of Na^+ and under physiological membrane potentials, the voltage-dependent sodium channel is responsible for loading the alkali ion into the EBCs.

Bladder ClC Transporters Mediate Chloride Sequestration into Vacuoles

We predict that the cytosolic Na^+ and Cl^- level is about 10 mM in the cytoplasm of epidermal cells (ECs) and about 1 M in EBC

vacuoles [26]. To accomplish a 100-fold accumulation of salt, a transmembrane pH gradient of at least 2 and an uphill Na^+ and Cl^- transport coupled to the PMF of downhill (lumen to cytosol) movement of protons is required. We tested this prediction for the bladder-expressed CqClC-c-mediated transport of chloride into the vacuole.

Archetypical ClC-type transport systems either operate as chloride channels or Cl^-/H^+-antiporters [27, 28]. In plants, however, ClCs use the PMF to accumulate nitrate in the vacuole [29].

We found 23 ClC homologs, 13 of which were differentially expressed in EBCs (7 transcripts) and leaves (6 transcripts; Data S2C). The quinoa ClC-c ortholog was analyzed via qPCR, and the resulting expression pattern confirmed the RNA-seq observation. CqClC-c shows a higher transcript level in bladders compared to leaves (Figure S4A). To validate the vacuole localization of CqClC-c *in planta*, we transiently expressed a GFP:CqClC-c construct in mesophyll protoplasts isolated from *Arabidopsis thaliana clca-2* mutant plants [29]. Confocal imaging of released vacuoles revealed CqClC-c localization at the tonoplast (Figure 3A). Because salt sequestration into EBC vacuoles requires a transport system for chloride, we investigated the ion selectivity of CqClC-c and compared it to NO_3^-/H^+-exchanger AtClC-a [29]. To study the function of CqClC-c, the transporter was expressed in mesophyll protoplasts from an *Arabidopsis* mutant lacking ClC-type vacuole anion current [29]. The ClC mutant was transiently transformed with GFP:AtClC-a or GFP:CqClC-c, and anion currents were studied in the whole-vacuolar patch clamp. In symmetric chloride conditions, depolarizing and hyperpolarizing voltage pulses elicited typical ClC-type inward and outward currents (Figures 3B, 3C, and S3C, red), resulting in a vacuolar current density (I_D) of $\sim$80 pA/pF (Figures 3D and S3B). This documents that CqClC-c can complement the mutant lacking the major *Arabidopsis* vacuole ClC. Changing cytosolic chloride to gluconate (impermeable to ClCs) abolished the negative (anion efflux from cytosol), but not the positive (anion influx into the cytosol), current components for AtClC-a-expressing vacuoles [30]. For CqClC-c also, the positive currents decreased, which indicates that cytosolic Cl^- is required for CqClC-c transport function (Figures 3B, 3C, and S3C, gray). Interestingly, differences in the current amplitude and V_{rev} could be observed in presence of either cytosolic NO_3^- or Cl^- conditions between the *Arabidopsis* and the quinoa protein (Figures 3B, 3C, and S3C, blue and red; Table 1). This difference in the V_{rev} (measure for transporter selectivity) for AtClC-a and CqClC-c indicates a strong chloride selectivity for the quinoa transporter. The anion preference of ClC-type transporters is correlated to the presence of a serine or proline in the selectivity filter. The amino acid sequence of AtClC-a contains a proline at position 160, a critical residue for determining nitrate or chloride selectivity [31]. CqClC-c carries a serine residue (S172) at the corresponding position, which most likely results in a higher conductivity for Cl^- compared to NO_3^-. This altered selectivity allows CqClC-c to fulfill its function in the chloride sequestration into the vacuole of EBCs.

Potassium and Proline Import Keeps the Bladder Cytoplasm Osmotically Balanced

Given that under saline conditions, up to 1 M NaCl is found in EBCs, a pronounced salt gradient must exist between the
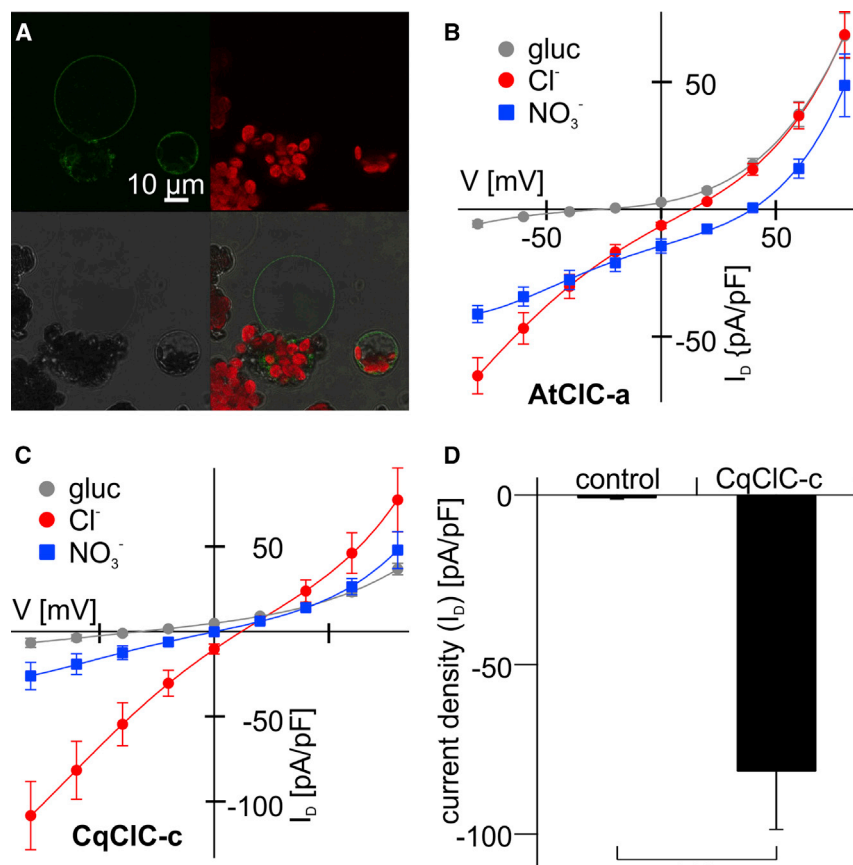
Figure 3. Quinoa ClC-c Targets to the Tono-plast and Displays a Different Anion Selectivity Than AtClC-a

(A) Confocal images of a GFP-positive vacuole showing expression of CqClC-c on the tonoplast. Top left: green fluorescence of GFP:CqClC-c at the tonoplast; top right: red chlorophyll auto-fluorescence of isolated chloroplasts; bottom left: bright field; bottom right: overlay.

(B and C) Average steady-state currents (normalized to membrane capacitance) of *Arabidopsis* vacuoles transiently expressing GFP-AtClC-a (B) or GFP-CqClC-c (C) in cytosolic gluconate (gluc), chloride, and nitrate.

(D) Summary plot of current densities recorded at −60 mV in untransformed (control) and GFP-tagged vacuoles (CqClC-c; mean ± SEM; n = 5; ***p < 0.001).

See also Figure S4.

bladder apoplast and cytoplasm on one side and cytoplasm and vacuole on the other [26]. To maintain the membrane potential, cytoplasmic homeostasis, and cell turgor, plants under salt stress need to take up K$^+$ as well [32–35]. Such salt-induced increases in K$^+$ concentration have also been observed with bladders [8].

Apart from voltage-gated Shaker-type potassium channels [36], plants use high-affinity K$^+$ transporters for K$^+$ acquisition [37]. The latter transporter type energizes high-affinity K$^+$ uptake by coupling uphill transport of potassium to the downhill flux of protons [38]. Pumping H$^+$ out of the EBC (for H$^+$ ATPases expression, see Data S2E) generates an inward-directed 2-fold pH gradient and hyperpolarizes the PM potential to approximately −120 mV [26]. Together, this driving force is used to power bladder PM solute transport. Potassium transporters from the HAK/KUP/KT family take advantage of this PMF to energize their K$^+$ transport when activated by the calcium sensor-kinase complex CBL1/9-CIPK23 [38, 39]. In quinoa, four proteins of the HAK/KUP/KT family could be found, which share a homology of ≥48% to each other. Among them, two were differentially expressed in EBCs when compared to roots (Data S2C; Figure 4A). When CqHAK (Data S2C) carrying a mOrange tag was transiently transformed into *Arabidopsis* protoplasts, fluorescence was found to be associated with the PM (Figure S5A). To study the function of the quinoa transporter, we expressed CqHAK together with CIPK23-CBL1 in oocytes and characterized electrical properties of the PM protein using the two-electrode voltage-clamp technique (Figure 4B). Macroscopic inward

currents were only observed when the transport protein was co-expressed with the calcium sensor-kinase complex (Figure 4B). When the external media was buffered to pH 7 or pH 5.5 and the PM clamped to −120 mV (a potential that reflects the resting potential of EBCs), no or only very small inward currents were observed in CqHAK/CIPK23/CBL1-expressing oocytes compared to control cells (Figure 4C, left). A proton-gradient-dependent activation of CqHAK was observed by decreasing the external pH to 4. In the presence of 2 mM KCl at pH 4 in the bath solution, changes in membrane potential were followed by either a decrease or an increase in K$^+$ influx (Figures S5B and S5C). Increasing external K$^+$ concentration caused the inward currents to rise in a fashion that could be fitted by a Michaelis-Menten equation, resulting in a high-affinity K$_m$ value of ∼50 μM for K$^+$ (Figure 4D). After replacement of 2 mM K$^+$ by Na$^+$ of the same concentration, inward currents ceased, indicating that Na$^+$ does not provide a substrate for transporters of the HAK/KUP/KT family (Figure 4C, right).

In addition to K$^+$, the movement of salt across the cytoplasmic layer of the EBC into the huge vacuole is very likely buffered by the production or uptake of compatible osmolytes. These osmoprotectants shield the cytoplasmic metabolism from the toxic effects of salt traveling through [20].

Plant osmoprotectants are classified by their chemical compound classes into three major groups: amino acids; polyol and/or sugars (Data S2F); and quaternary amines [8, 40]. Metabolic profiling identified proline as a major bladder osmolyte [8]. Proline in the chloroplast is made from glutamate. EBCs and mesophyll cells contain an equal number of chloroplasts in comparison (Table S2). However, considering an ∼27 times larger volume of a single EBC compared to a mesophyll cell (with a cytosolic volume of 18% for EBCs and 31% for mesophyll cells), one can suggest a relatively low biosynthetic activity in bladders (Data S1A). Pyrroline-carboxylate synthase transcript (P5CS2) in EBCs is much lower than in leaves, suggesting

Table 1. V$_{rev}$ of Vacuolar ClC-c Currents in Various Anion Conditions

	Arabidopsis AtClC-a	Quinoa CqClC-c
Gluconate	−30 ± 5 (3)	−40 ± 10 (5)
Chloride	13 ± 1 (3)	12 ± 1 (5)
Nitrate	39 ± 1 (3)	0.3 ± 1.1 (5)

V$_{rev}$ of AtClC-a or CqClC-c-expressing vacuoles in different anion solutions applied on the cytosolic side, whereas chloride on the vacuolar side was constant. V$_{rev}$ (in mV) was calculated from current-voltage (IV) relationships (mean ± SEM). In parentheses are the numbers of investigated vacuoles.

increased proline synthesis occurs in response to salt in leaves (Figures S6A and S6B; Data S2F). Searching for proline transporters [41, 42], we found four ProT homologs in quinoa that are upregulated in leaves at the transcript level but did not alter their expression by salt (Data S2F). Together, this suggests that the rate-limiting step of proline accumulation in EBCs is not transport but salt-dependent synthesis in leaves.

Given that quinoa leaves act as proline factories, we were interested in the proline transport into EBCs mediated by CqProT-type transporters. We identified and cloned a quinoa ProT, for which qPCR analysis revealed 18-fold higher transcript levels in bladder compared to leaves (Figure 5A). When mOrange:CqProT constructs were transiently expressed in *Arabidopsis* protoplasts, fluorescence was emitted from the PM (Figure S6C). To characterize the proline-associated functional properties of the putative compatible osmolyte transporter, we expressed CqProT in *Xenopus* oocytes. When ProT-expressing oocytes were placed in media with pH 7 and exposed to proline, no induction of an electrical activity was observed compared to control oocytes. However, proline application at pH 5.5, and even more at pH 4, elicited inward currents of −30 nA and −200 nA, respectively (Figure 5B). At the same time, under acidic external conditions, the membrane potential was depolarized, indicating that CqProT utilizes the PMF to drive proline accumulation in EBCs (Figure 5C) [41, 43, 44]. Replacing proline by the stress-related metabolite γ-aminobutyric acid (GABA) indicated that GABA is transported by CqProT too (Figure 5D).

DISCUSSION

Until now, most studies on salt bladders have been conducted using the inducible CAM plant *Mesembryanthemum crystallinum* [6, 45, 46]. However, the genome of this CAM plant is unknown and thus genetics rather limited. From both physiological and biochemical points of view, *M. crystallinum* is unusual, harboring unique features that are rarely found in any crop, such as pronounced succulence and a transition from C3 to CAM metabolism under salt stress [5]. In contrast, quinoa offers an ideal alternative model for studying plant salt tolerance mechanisms, as quinoa is sequenced already, considered as a pseudo-cereal crop [47], and closely related to several other important *Amaranthaceae* crops (e.g., spinach, sugar beet, and chard), facilitating translational research.

In this study, we have identified genes encoding membrane transporters that are differentially expressed in quinoa EBCs.

For salt to enter and accumulate in the vacuole of the salt dumpers, the Na$^+$ and Cl$^-$ need to pass through membranes and travel to the bladder cytoplasm. To gain elements relevant for a working model, we considered differentially expressed genes (DEGs), including transporters in general and those that have been shown associated with salt management in *Arabidopsis* in particular. Based on the membrane localization of well-known transport protein orthologs, thermodynamics considerations, and functional properties of the bladder membrane, the associated elements for a polar salt transport scheme were drawn (Figures 6A and 6B).

### Bladder Transport Modules Come Hard Wired

RNA-seq analysis of leaf and bladder samples (i.e., L+/L−B+/B comparison) revealed only a small number (83) of genes showing responses to salt. Because of the relatively small number of significant changes in transcript levels under salt for most transporter genes, one could suggest that bladder cells are "constitutively active" in salt sequestration and that the transcript level responses of transporters only play a minor role under salt stress. However, this lack of transcript level salt stress regulation may not mean a constitutive function of proteins because many transporters are regulated and activated at a posttranslational level. The finding that the calcium sensor-kinase complex of CBL/CIPK type is differentially expressed and required to activate CqHAK (Figure 4) in EBCs might indicate that salt dumpers are under control of the salt-stress-induced calcium signaling pathway.

Voltage-Dependent and Strictly Na$^+$-Selective HKT1.2: a One-Way Sodium Path into the Bladder

Quinoa has two HKT1 genes: CqHKT1.1 (expressed in roots) and CqHKT1.2 (in leaves and EBCs). Unlike the root CqHKT1.1, the bladder-expressed CqHKT1.2 represents an inward-rectifying sodium channel (Figures 2 and S3). Bladders from the ice plant *Mesembryanthemum crystallinum* also express a CqHKT1.2 ortholog [23], which mediates voltage-dependent sodium influx (Figure S3; c.f. a rice HKT1) [48, 49]. For quinoa, the consistency in the bladder location and specific function supports the notion that CqHKT1.2 allows Na$^+$ to pass into the salt dumpers (Figure 6A). When large quantities of the positively charged Na$^+$ enter the cell, the NHX-type transporter cannot move Na$^+$ toward the lumen of the central storage organ at sufficient speed, and sodium would accumulate and reach cytotoxic levels. When the membrane depolarizes, the CqHKT1.2 channel's gate closes, preventing Na$^+$ influx but more important also efflux at the same time. This can be seen as a safety mechanism to avoid overloading the cytoplasm with Na$^+$. At the same time, under conditions when the membrane voltage drops below the electrochemical potential of Na$^+$, the closed CqHKT1.2 channel prevents Na$^+$ leakage from the EBC.

All plants, including halophytes, take advantage of a salt-sensing and SOS1 retrieval system. The EBCs, in an agreement with their salt dumper function, do not express a SOS1-type sodium export mechanism (Data S2C and S2D) but instead possess CqHKT1.2, a voltage-dependent sodium channel for predominantly one-way Na$^+$ entry.

Considering that NaCl is the dominant salt in saline soils, the question of how chloride is transported across the PM of EBCs
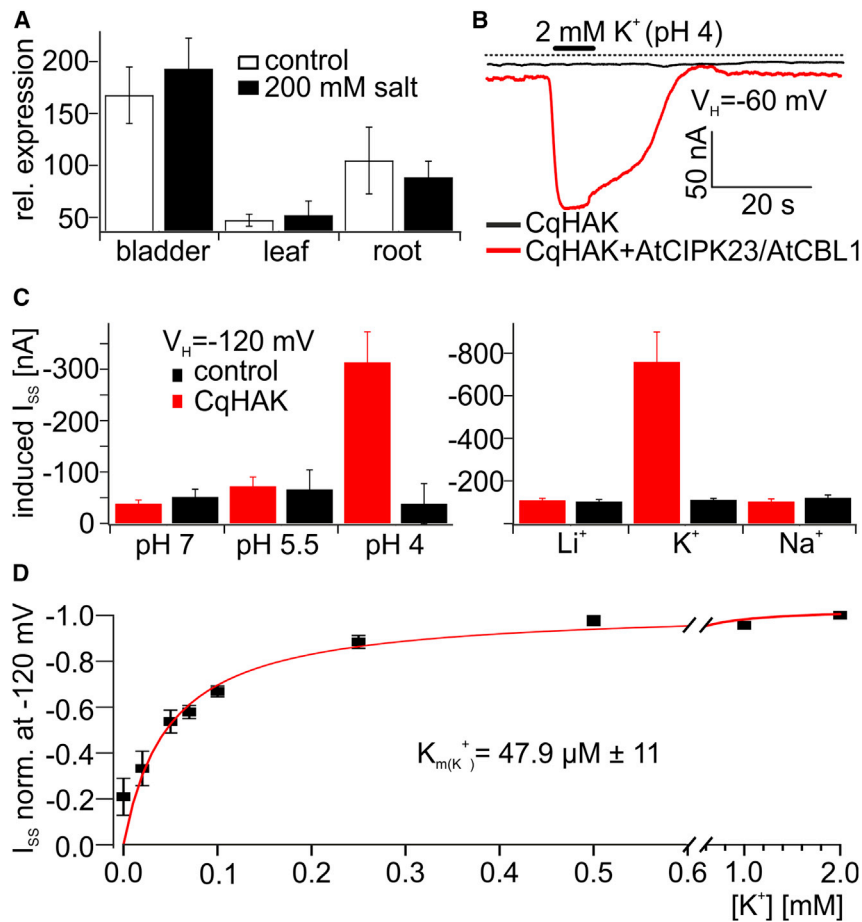
Figure 4. Quinoa HAK-like Transporters Share the Electrophysiological Characteristics of the HAK/KUP/KT Family

(A) qPCR of a HAK-like transporter, which is highly expressed in EBC and insensitive to salt (mean ± SE; n ≥ 7).

(B) Whole-oocyte currents of a control and CqHAK/AtCIPK23/AtCBL1-expressing oocyte. Addition of K$^+$ resulted in macroscopic inward currents only in CqHAK/AtCIPK23/AtCBL1-expressing oocytes. The dotted line represents zero current.

(C) Current recordings of control or CqHAK/AtCIPK23/AtCBL1-injected oocytes. Left: I$_{SS}$ in response to different pH conditions and 2 mM K$^+$. Compared with control oocytes, K$^+$ currents increased at pH 4 (mean ± SD; n = 5). Right: only the application of K$^+$ resulted in macroscopic inward currents, whereas in Li$^+$ or Na$^+$, no current response was induced (2 mM each; mean ± SD; n = 4).

(D) Dose-response curve of CqHAK/AtCIPK23/AtCBL1-expressing oocytes. The Michaelis-Menten fit revealed a K$_{m(K^+)}$ value of 47.90 μM (mean ± SD; n = 6).

See also Figure S5 and Data S2.

arises. One possibility that should be addressed in future approaches is that members of the NPF transporter super-family may be involved. NPF proteins in general are described to transport a huge variety of substrates, including anions [50]. One member, NPF2.4, was recently found to be permeable for chloride. Although NPF2.4 seems to be involved in the Cl$^-$ xylem loading in roots [51], it is tempting to speculate that further members of the family could be permeable for Cl$^-$ in preference to NO$_3^-$. With this assumption, NPFs could still be candidates to transport Cl$^-$ across the PM, maybe also with a one-way path for chloride.

A ClC-type Transporter Facilitates Chloride Movement into the EBC Vacuole

ClC-type proteins are ubiquitously found in eukaryotes and prokaryotes, and plant members are described as either anion channels or anion/H$^+$ antiporters [27, 28]. The best described plant ClC (AtClC-a) is involved in nitrate homeostasis due to the translocation of nitrate into the vacuole, whereas AtClC-c mutant plants exhibit a role of this transporter in the chloride movement under salt stress conditions [52]. The quinoa RNA-seq data showed an ortholog of AtClC-c that is expressed at higher levels in bladders than leaves. The expression pattern, the localization at the tonoplast, and the chloride-mediated transport activity (Figures 3 and S4) together indicate a function for CqClC-c in chloride accumulation in EBC vacuoles. To pro-

vide consistent transport of chloride into the vacuole, we predict a Cl$^-$/H$^+$-mediated antiport activity for CqClC-c. The PMF at the tonoplast, which is generated by ATP- and PPi-fuelled vacuolar pumps, would allow chloride accumulation under dramatically increasing chloride concentrations in the vacuole. Evidence for function of CqClC-c as an antiporter could be found in the amino acid sequence. The crystal structure of the bacterial CLC-ec1 protein shows two conserved glutamates (E148 and E203) [53], which are key residues for ion transport. E203 is conserved in all ClC-type antiporters, whereas ClC-type channels exhibit a valine at the corresponding position [54]. The CqClC-c sequence shows two glutamates at corresponding positions, E215 and E282. This leads us to the suggestion that CqClC-c acts as a Cl$^-$/H$^+$ antiporter and utilizes the PMF to sequester chloride into the EBC vacuole (Figure 6A).

Salt Sequestration Needs to be Balanced by Osmolytes

Potassium is the major cationic osmolyte in the cytoplasm. For bladders to grow and develop, they, like any plant cell from non-halophytes, need to take up K$^+$. The bladders express a HAK-type high-affinity K$^+$ transporter (Figure 4). In non-halophytes, such as *Arabidopsis*, HAK5 is expressed under K$^+$ starvation and saline conditions [55, 56]. If plants are exposed to high extracellular Na$^+$ concentration and simultaneously have limited access to K$^+$, a member of the HAK/KUP/KT family takes action. The bladder-expressed HAK-like protein transports K$^+$, but not Na$^+$, by coupling the uphill flux of K$^+$ to the downhill flux of protons (Figure 6B).

Furthermore, under salt stress, compatible osmolytes play an important role to protect the cytosolic metabolism from the toxic effect of NaCl. Recent metabolomics data showed an increase of
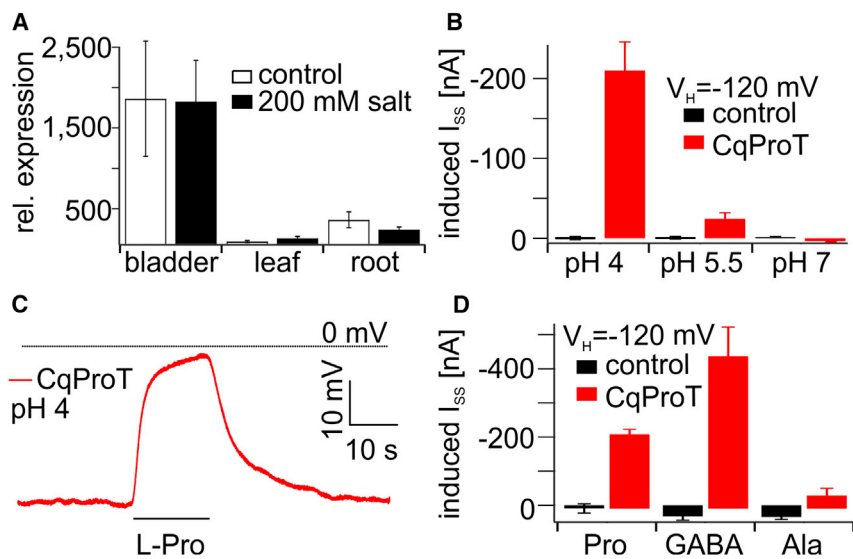
Figure 5. The Proline Transporter CqProT Mediates Compatible Solute Transport into EBCs

(A) CqProT is high expressed in EBCs compared to leaf and root and independent of salt (mean ± SE; $n \geq 7$).

(B) Compared to control oocytes, CqProT-expressing oocytes exhibit substrate-induced inward currents in 20 mM L-proline that increased with an external acidification (mean ± SD; $n = 4$).

(C) 20 mM L-proline triggers the depolarization of the oocyte membrane at pH 4. The dotted line represents 0 mV.

(D) Substrate-induced currents of control and CqProT-expressing oocytes in 20 mM Pro, GABA, and Ala. The presence of Pro or GABA resulted in macroscopic inward currents (mean ± SD; $n = 4$). See also Figure S6 and Data S2.

proline under salt stress conditions [8]. Given that RNA-seq data revealed that leaves could act as proline factories, we focused on the possible transport of proline across the PM into the EBCs (Figure 6B). We have shown that bladders express a ProT-type transporter, which mediates a proton-driven proline uptake (Figure 5). Interestingly, CqProT also transports the stress-related GABA, which is known to have effects on plant channel activity [26, 57]. It was speculated that an increased

accumulation of GABA in EBCs could feed back on the rate of salt loading in EBCs [8]. So one could suggest that CqProT not only plays a role in providing the osmolyte proline but also bringing the ion transport under control of GABA [57, 58] (c.f. action of GABA in guard cells).

In summary, our characterization of the expression profiles and functional features of genes relevant for salt management helps to explain how salt bladders may function as salt
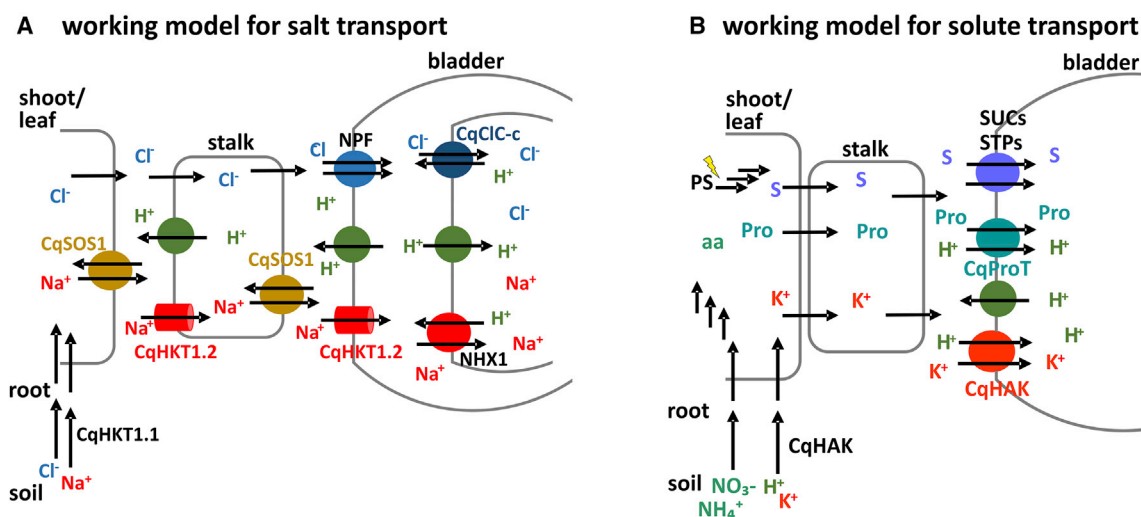
Figure 6. A Working Model of Bladder Transport Systems

(A) The red and yellow pathway illustrates the Na^+ transport module via CqHKT1.2 and CqSOS1 from the soil into the EBC. Especially CqHKT1.2 channels mediate a one-way Na^+ transport that is directed to EBCs due to its electrophysiological properties. The Na^+ transport by CqSOS1 requires the PMF, which is established by ATPases (green). The counterion chloride (blue) could be loaded into EBCs by the PM- and tonoplast-located transporters NPFs and CqClC-c, respectively.

(B) The solute transport from leaves to EBCs is required to provide energy and osmotic balance in the EBCs. Due to the low photosynthetic activity of EBCs, these cells are dependent on the energy import from the leaf, which could be mediated by sugar transporters, like SUCs and SWEETs (light purple). Furthermore, nitrogen from the soil is metabolized in the leaf, and the resulting compatible osmolytes (like proline) are transported to the sink tissue by the Pro/H^+ symporter CqProT (cyan). Besides proline, potassium is also transported via the K^+/H^+ symporter CqHAK into EBCs for osmolyte-balancing purposes (red). See also Table S1 and Data S1 and S2.

dumpers to confer salt tolerance to quinoa and other bladder-bearing halophytes. Central to our working model is the one-way movement of Na$^+$ across the bladder PM mediated by CqHKT1.2 and Cl$^-$ transport via CqClC-c. We find that CqProT and CqHAK contribute to the accumulation of the compatible osmolytes proline and K$^+$, respectively, in the cytoplasm of EBCs. A recently published paper used the quinoa draft genome to identify the first quinoa mutant, induced by ethyl methanesulfonate (EMS) mutagenesis [59]. This is a game-changing resource for future research on the naturally salt-tolerant halophyte and could be used to build on the presented working model for bladder-based salt sequestration in future approaches.

STAR★METHODS

Detailed methods are provided in the online version of this paper and include the following:

- KEY RESOURCES TABLE
- CONTACT FOR REAGENT AND RESOURCE SHARING
- EXPERIMENTAL MODEL AND SUBJECT DETAILS
  - ○ Plant material and growth conditions
  - ○ *Xenopus* oocyte preparation
- METHOD DETAILS
  - ○ RNA extraction
  - ○ RNA-sequencing and data analysis
  - ○ cDNA preparation and expression analyses
  - ○ Cloning and cRNA synthesis
  - ○ Protoplast isolation and transformation
  - ○ Electron microscopy
  - ○ Confocal microscopy
  - ○ Oocyte recordings
  - ○ Patch-clamp recordings
  - ○ Alignment and phylogenetic analysis of CqHKTs
- QUANTIFICATION AND STATISTICAL ANALYSIS
- DATA AND SOFTWARE AVAILABILITY

SUPPLEMENTAL INFORMATION

Supplemental Information includes six figures, three tables, and two data files and can be found with this article online at https://doi.org/10.1016/j.cub.2018.08.004.

AUTHOR CONTRIBUTIONS

K.F.X.M., S. Shabala, K.A.S.A.-R., G.H., H.Z., J.-K.Z., and R.H. designed research; J.B., M.M., H.M.M., S. Scherzer, N.B., C.S., T.M., J.S.-S., and A.G. performed research; J.B., H.M.M., S. Scherzer, T.M., C.S., A.C., P.A., and H.Z. analyzed data; M.M., K.F.X.M., and G.H. performed bioinformatic analysis; and J.B., M.M., H.M.M., S. Shabala, G.H., J.-K.Z., and R.H. wrote the paper.

REFERENCES

1. Jacobsen, S.-E., Mujica, A., and Jensen, C.R. (2003). The resistance of quinoa (*Chenopodium quinoa* Willd.) to adverse abiotic factors. Food Rev. Int. *19*, 99–109.

2. Jarvis, D.E., Ho, Y.S., Lightfoot, D.J., Schmöckel, S.M., Li, B., Borm, T.J., Ohyanagi, H., Mineta, K., Michell, C.T., Saber, N., et al. (2017). The genome of *Chenopodium quinoa*. Nature *542*, 307–312.

3. Yasui, Y., Hirakawa, H., Oikawa, T., Toyoshima, M., Matsuzaki, C., Ueno, M., Mizuno, N., Nagatoshi, Y., Imamura, T., Miyago, M., et al. (2016). Draft genome sequence of an inbred line of *Chenopodium quinoa*, an allotetraploid crop with great environmental adaptability and outstanding nutritional properties. DNA Res. *23*, 535–546.

4. Zou, C., Chen, A., Xiao, L., Müller, H.M., Ache, P., Haberer, G., Zhang, M., Jia, W., Deng, P., Huang, R., et al. (2017). A high-quality genome assembly of quinoa provides insights into the molecular basis of salt bladder-based salinity tolerance and the exceptional nutritional value. Cell Res. *27*, 1327–1340.

5. Adams, P., Nelson, D.E., Yamada, S., Chmara, W., Jensen, R.G., Bohnert, H.J., and Griffiths, H. (1998). Growth and development of *Mesembryanthemum crystallinum* (Aizoaceae). New Phytol. *138*, 171–190.

6. Oh, D.H., Barkla, B.J., Vera-Estrella, R., Pantoja, O., Lee, S.Y., Bohnert, H.J., and Dassanayake, M. (2015). Cell type-specific responses to salinity - the epidermal bladder cell transcriptome of *Mesembryanthemum crystallinum*. New Phytol. *207*, 627–644.

7. Adams, P., Thomas, J.C., Vernon, D.M., Bohnert, H.J., and Jensen, R.G. (1992). Distinct cellular and organismic responses to salt stress. Plant Cell Physiol. *33*, 1215–1223.

8. Kiani-Pouya, A., Roessner, U., Jayasinghe, N.S., Lutz, A., Rupasinghe, T., Bazihizina, N., Bohm, J., Alharbi, S., Hedrich, R., and Shabala, S. (2017). Epidermal bladder cells confer salinity stress tolerance in the halophyte quinoa and Atriplex species. Plant Cell Environ. *40*, 1900–1915.

9. Bauer, H., Ache, P., Lautner, S., Fromm, J., Hartung, W., Al-Rasheid, K.A., Sonnewald, S., Sonnewald, U., Kneitz, S., Lachmann, N., et al. (2013). The stomatal response to reduced relative humidity requires guard cell-autonomous ABA synthesis. Curr. Biol. *23*, 53–57.

10. Cui, H., Zhang, S.T., Yang, H.J., Ji, H., and Wang, X.J. (2011). Gene expression profile analysis of tobacco leaf trichomes. BMC Plant Biol. *11*, 76.

11. Jakoby, M.J., Falkenhan, D., Mader, M.T., Brininstool, G., Wischnitzki, E., Platz, N., Hudson, A., Hülskamp, M., Larkin, J., and Schnittger, A. (2008). Transcriptional profiling of mature *Arabidopsis* trichomes reveals that NOECK encodes the MIXTA-like transcriptional regulator MYB106. Plant Physiol. *148*, 1583–1602.

12. Yoo, M.J., Ma, T., Zhu, N., Liu, L., Harmon, A.C., Wang, Q., and Chen, S. (2016). Genome-wide identification and homeolog-specific expression analysis of the SnRK2 genes in *Brassica napus* guard cells. Plant Mol. Biol. *91*, 211–227.

13. Bemm, F., Becker, D., Larisch, C., Kreuzer, I., Escalante-Perez, M., Schulze, W.X., Ankenbrand, M., Van de Weyer, A.L., Krol, E., Al-Rasheid, K.A., et al. (2016). Venus flytrap carnivorous lifestyle builds on herbivore defense strategies. Genome Res. *26*, 812–825.

14. Daum, B., Nicastro, D., Austin, J., 2nd, McIntosh, J.R., and Kühlbrandt, W. (2010). Arrangement of photosystem II and ATP synthase in chloroplast membranes of spinach and pea. Plant Cell *22*, 1299–1312.

15. Shi, H., Quintero, F.J., Pardo, J.M., and Zhu, J.K. (2002). The putative plasma membrane Na$^+$/H$^+$ antiporter SOS1 controls long-distance Na$^+$ transport in plants. Plant Cell *14*, 465–477.

16. Waters, S., Gilliham, M., and Hrmova, M. (2013). Plant high-affinity potassium (HKT) transporters involved in salinity tolerance: structural insights to probe differences in ion selectivity. Int. J. Mol. Sci. *14*, 7660–7680.

17. Qiu, Q.S., Guo, Y., Dietrich, M.A., Schumaker, K.S., and Zhu, J.K. (2002). Regulation of SOS1, a plasma membrane Na$^+$/H$^+$ exchanger in *Arabidopsis thaliana*, by SOS2 and SOS3. Proc. Natl. Acad. Sci. USA *99*, 8436–8441.

18. Quintero, F.J., Ohta, M., Shi, H., Zhu, J.K., and Pardo, J.M. (2002). Reconstitution in yeast of the *Arabidopsis* SOS signaling pathway for Na$^+$ homeostasis. Proc. Natl. Acad. Sci. USA *99*, 9061–9066.

19. Shi, H., Ishitani, M., Kim, C., and Zhu, J.K. (2000). The *Arabidopsis thaliana* salt tolerance gene SOS1 encodes a putative Na$^+$/H$^+$ antiporter. Proc. Natl. Acad. Sci. USA *97*, 6896–6901.

20. Shabala, S., and Mackay, A. (2011). Chapter 5 - Ion transport in halophytes. Adv. Bot. Res. *57*, 151–199.

21. Arabbeigi, M., Arzani, A., Majidi, M.M., Sayed-Tabatabaei, B.E., and Saha, P. (2018). Expression pattern of salt tolerance-related genes in *Aegilops cylindrica*. Physiol. Mol. Biol. Plants *24*, 61–73.

22. Mishra, S., Singh, B., Panda, K., Singh, B.P., Singh, N., Misra, P., Rai, V., and Singh, N.K. (2016). Association of SNP haplotypes of HKT family genes with salt tolerance in Indian wild rice germplasm. Rice (N. Y.) *9*, 15.

23. Platten, J.D., Cotsaftis, O., Berthomieu, P., Bohnert, H., Davenport, R.J., Fairbairn, D.J., Horie, T., Leigh, R.A., Lin, H.X., Luan, S., et al. (2006). Nomenclature for HKT transporters, key determinants of plant salinity tolerance. Trends Plant Sci. *11*, 372–374.

24. Böhm, J., Scherzer, S., Shabala, S., Krol, E., Neher, E., Mueller, T.D., and Hedrich, R. (2016). Venus flytrap HKT1-type channel provides for prey sodium uptake into carnivorous plant without conflicting with electrical excitability. Mol. Plant *9*, 428–436.

25. Lefoulon, C., Karnik, R., Honsbein, A., Gutla, P.V., Grefen, C., Riedelsberger, J., Poblete, T., Dreyer, I., Gonzalez, W., and Blatt, M.R. (2014). Voltage-sensor transitions of the inward-rectifying K$^+$ channel KAT1 indicate a latching mechanism biased by hydration within the voltage sensor. Plant Physiol. *166*, 960–975.

26. Shabala, S., Bose, J., and Hedrich, R. (2014). Salt bladders: do they matter? Trends Plant Sci. *19*, 687–691.

27. Accardi, A., and Picollo, A. (2010). CLC channels and transporters: proteins with borderline personalities. Biochim. Biophys. Acta *1798*, 1457–1464.

28. Zifarelli, G., and Pusch, M. (2010). CLC transport proteins in plants. FEBS Lett. *584*, 2122–2127.

29. De Angeli, A., Monachello, D., Ephritikhine, G., Frachisse, J.M., Thomine, S., Gambale, F., and Barbier-Brygoo, H. (2006). The nitrate/proton antiporter AtCLCa mediates nitrate accumulation in plant vacuoles. Nature *442*, 939–942.

30. Carpaneto, A., Boccaccio, A., Lagostena, L., Di Zanni, E., and Scholz-Starke, J. (2017). The signaling lipid phosphatidylinositol-3,5-bisphosphate targets plant CLC-a anion/H$^+$ exchange activity. EMBO Rep. *18*, 1100–1107.

31. Wege, S., Jossier, M., Filleur, S., Thomine, S., Barbier-Brygoo, H., Gambale, F., and De Angeli, A. (2010). The proline 160 in the selectivity filter of the *Arabidopsis* NO$_3^-$/H$^+$ exchanger AtCLCa is essential for nitrate accumulation in planta. Plant J. *63*, 861–869.

32. Al Hassan, M., Estrelles, E., Soriano, P., López-Gresa, M.P., Bellés, J.M., Boscaiu, M., and Vicente, O. (2017). Unraveling salt tolerance mechanisms in halophytes: a comparative study on four Mediterranean *Limonium* species with different geographic distribution patterns. Front. Plant Sci. *8*, 1438.

33. Hariadi, Y., Marandon, K., Tian, Y., Jacobsen, S.E., and Shabala, S. (2011). Ionic and osmotic relations in quinoa (*Chenopodium quinoa* Willd.) plants grown at various salinity levels. J. Exp. Bot. *62*, 185–193.

34. Pan, Y.Q., Guo, H., Wang, S.M., Zhao, B., Zhang, J.L., Ma, Q., Yin, H.J., and Bao, A.K. (2016). The photosynthesis, Na$^+$/K$^+$ homeostasis and osmotic adjustment of *Atriplex canescens* in response to salinity. Front. Plant Sci. *7*, 848.

35. Tada, Y., Komatsubara, S., and Kurusu, T. (2014). Growth and physiological adaptation of whole plants and cultured cells from a halophyte turf grass under salt stress. AoB Plants *6*, plu041.

36. Hedrich, R. (2012). Ion channels in plants. Physiol. Rev. *92*, 1777–1811.

37. Kim, E.J., Kwak, J.M., Uozumi, N., and Schroeder, J.I. (1998). AtKUP1: an *Arabidopsis* gene encoding high-affinity potassium transport activity. Plant Cell *10*, 51–62.

38. Scherzer, S., Böhm, J., Krol, E., Shabala, L., Kreuzer, I., Larisch, C., Bemm, F., Al-Rasheid, K.A., Shabala, S., Rennenberg, H., et al. (2015). Calcium sensor kinase activates potassium uptake systems in gland cells of Venus flytraps. Proc. Natl. Acad. Sci. USA *112*, 7309–7314.

39. Ragel, P., Ródenas, R., García-Martín, E., Andrés, Z., Villalta, I., Nieves-Cordones, M., Rivero, R.M., Martínez, V., Pardo, J.M., Quintero, F.J., and Rubio, F. (2015). The CBL-interacting protein kinase CIPK23 regulates HAK5-mediated high-affinity K$^+$ uptake in *Arabidopsis* roots. Plant Physiol. *169*, 2863–2873.

40. Khan, M.S., Ahmad, D., and Khan, M.A. (2015). Utilization of genes encoding osmoprotectants in transgenic plants for enhanced abiotic stress tolerance. Electron. J. Biotechnol. *18*, 257–266.

41. Rentsch, D., Hirner, B., Schmelzer, E., and Frommer, W.B. (1996). Salt stress-induced proline transporters and salt stress-repressed broad specificity amino acid permeases identified by suppression of a yeast amino acid permease-targeting mutant. Plant Cell *8*, 1437–1446.

42. Grallath, S., Weimar, T., Meyer, A., Gumy, C., Suter-Grotemeyer, M., Neuhaus, J.M., and Rentsch, D. (2005). The AtProT family. Compatible solute transporters with similar substrate specificity but differential expression patterns. Plant Physiol. *137*, 117–126.

43. Igarashi, Y., Yoshiba, Y., Takeshita, T., Nomura, S., Otomo, J., Yamaguchi-Shinozaki, K., and Shinozaki, K. (2000). Molecular cloning and characterization of a cDNA encoding proline transporter in rice. Plant Cell Physiol. *41*, 750–756.

44. Schwacke, R., Grallath, S., Breitkreuz, K.E., Stransky, E., Stransky, H., Frommer, W.B., and Rentsch, D. (1999). LeProT1, a transporter for proline, glycine betaine, and gamma-amino butyric acid in tomato pollen. Plant Cell *11*, 377–392.

45. Barkla, B.J., and Vera-Estrella, R. (2015). Single cell-type comparative metabolomics of epidermal bladder cells from the halophyte *Mesembryanthemum crystallinum*. Front. Plant Sci. *6*, 435.

46. Barkla, B.J., Vera-Estrella, R., and Pantoja, O. (2012). Protein profiling of epidermal bladder cells from the halophyte *Mesembryanthemum crystallinum*. Proteomics *12*, 2862–2865.

47. Adolf, V.I., Jacobsen, S.-E., and Shabala, S. (2013). Salt tolerance mechanisms in quinoa (*Chenopodium quinoa* Willd.). Environ. Exp. Bot. *92*, 43–54.

48. Campbell, M.T., Bandillo, N., Al Shiblawi, F.R.A., Sharma, S., Liu, K., Du, Q., Schmitz, A.J., Zhang, C., Véry, A.A., Lorenz, A.J., and Walia, H. (2017). Allelic variants of OsHKT1;1 underlie the divergence between indica and japonica subspecies of rice (*Oryza sativa*) for root sodium content. PLoS Genet. *13*, e1006823.

49. Jabnoune, M., Espeout, S., Mieulet, D., Fizames, C., Verdeil, J.L., Conéjéro, G., Rodríguez-Navarro, A., Sentenac, H., Guiderdoni, E., Abdelly, C., and Véry, A.A. (2009). Diversity in expression patterns and functional properties in the rice HKT transporter family. Plant Physiol. *150*, 1955–1971.

50. Corratgé-Faillie, C., and Lacombe, B. (2017). Substrate (un)specificity of *Arabidopsis* NRT1/PTR FAMILY (NPF) proteins. J. Exp. Bot. *68*, 3107–3113.

51. Li, B., Byrt, C., Qiu, J., Baumann, U., Hrmova, M., Evrard, A., Johnson, A.A., Birnbaum, K.D., Mayo, G.M., Jha, D., et al. (2016). Identification of

a stelar-localized transport protein that facilitates root-to-shoot transfer of chloride in *Arabidopsis*. Plant Physiol. *170*, 1014–1029.

52. Jossier, M., Kroniewicz, L., Dalmas, F., Le Thiec, D., Ephritikhine, G., Thomine, S., Barbier-Brygoo, H., Vavasseur, A., Filleur, S., and Leonhardt, N. (2010). The *Arabidopsis* vacuolar anion transporter, AtCLCc, is involved in the regulation of stomatal movements and contributes to salt tolerance. Plant J. *64*, 563–576.

53. Dutzler, R., Campbell, E.B., Cadene, M., Chait, B.T., and MacKinnon, R. (2002). X-ray structure of a ClC chloride channel at 3.0 A reveals the molecular basis of anion selectivity. Nature *415*, 287–294.

54. Accardi, A., Walden, M., Nguitragool, W., Jayaram, H., Williams, C., and Miller, C. (2005). Separate ion pathways in a Cl⁻/H⁺ exchanger. J. Gen. Physiol. *126*, 563–570.

55. Gierth, M., Mäser, P., and Schroeder, J.I. (2005). The potassium transporter AtHAK5 functions in K⁺ deprivation-induced high-affinity K⁺ uptake and AKT1 K⁺ channel contribution to K⁺ uptake kinetics in *Arabidopsis* roots. Plant Physiol. *137*, 1105–1114.

56. Nieves-Cordones, M., Alemán, F., Martínez, V., and Rubio, F. (2010). The *Arabidopsis thaliana* HAK5 K⁺ transporter is required for plant growth and K⁺ acquisition from low K⁺ solutions under saline conditions. Mol. Plant *3*, 326–333.

57. Ramesh, S.A., Tyerman, S.D., Xu, B., Bose, J., Kaur, S., Conn, V., Domingos, P., Ullah, S., Wege, S., Shabala, S., et al. (2015). GABA signalling modulates plant growth by directly regulating the activity of plant-specific anion transporters. Nat. Commun. *6*, 7879.

58. Mekonnen, D.W., Flügge, U.-I., and Ludewig, F. (2016). Gamma-aminobutyric acid depletion affects stomata closure and drought tolerance of *Arabidopsis thaliana*. Plant Sci. *245*, 25–34.

59. Imamura, T., Takagi, H., Miyazato, A., Ohki, S., Mizukoshi, H., and Mori, M. (2018). Isolation and characterization of the betalain biosynthesis gene involved in hypocotyl pigmentation of the allotetraploid *Chenopodium quinoa*. Biochem. Biophys. Res. Commun. *496*, 280–286.

60. Nour-Eldin, H.H., Hansen, B.G., Nørholm, M.H.H., Jensen, J.K., and Halkier, B.A. (2006). Advancing uracil-excision based cloning towards an ideal technique for cloning PCR fragments. Nucleic Acids Res. *34*, e122.

61. Altschul, S.F., Madden, T.L., Schäffer, A.A., Zhang, J., Zhang, Z., Miller, W., and Lipman, D.J. (1997). Gapped BLAST and PSI-BLAST: a new generation of protein database search programs. Nucleic Acids Res. *25*, 3389–3402.

62. Sievers, F., Wilm, A., Dineen, D., Gibson, T.J., Karplus, K., Li, W., Lopez, R., McWilliam, H., Remmert, M., Söding, J., et al. (2011). Fast, scalable generation of high-quality protein multiple sequence alignments using Clustal Omega. Mol. Syst. Biol. *7*, 539.

63. Schäfer, N., Maierhofer, T., Herrmann, J., Jørgensen, M.E., Lind, C., von Meyer, K., Lautner, S., Fromm, J., Felder, M., Hetherington, A.M., et al. (2018). A tandem amino acid residue motif in guard cell SLAC1 anion channel of grasses allows for the control of stomatal aperture by nitrate. Curr. Biol. *28*, 1370–1379.e5.

64. Liao, Y., Smyth, G.K., and Shi, W. (2013). The Subread aligner: fast, accurate and scalable read mapping by seed-and-vote. Nucleic Acids Res. *41*, e108.

65. Liao, Y., Smyth, G.K., and Shi, W. (2014). featureCounts: an efficient general purpose program for assigning sequence reads to genomic features. Bioinformatics *30*, 923–930.

66. Robinson, M.D., McCarthy, D.J., and Smyth, G.K. (2010). edgeR: a Bioconductor package for differential expression analysis of digital gene expression data. Bioinformatics *26*, 139–140.

67. Grabherr, M.G., Haas, B.J., Yassour, M., Levin, J.Z., Thompson, D.A., Amit, I., Adiconis, X., Fan, L., Raychowdhury, R., Zeng, Q., et al. (2011). Full-length transcriptome assembly from RNA-seq data without a reference genome. Nat. Biotechnol. *29*, 644–652.

68. Thimm, O., Bläsing, O., Gibon, Y., Nagel, A., Meyer, S., Krüger, P., Selbig, J., Müller, L.A., Rhee, S.Y., and Stitt, M. (2004). MAPMAN: a user-driven tool to display genomics data sets onto diagrams of metabolic pathways and other biological processes. Plant J. *37*, 914–939.

69. Hooper, C.M., Tanz, S.K., Castleden, I.R., Vacher, M.A., Small, I.D., and Millar, A.H. (2014). SUBAcon: a consensus algorithm for unifying the subcellular localization data of the *Arabidopsis* proteome. Bioinformatics *30*, 3356–3364.

70. García-Alcalde, F., García-López, F., Dopazo, J., and Conesa, A. (2011). Paintomics: a web based tool for the joint visualization of transcriptomics and metabolomics data. Bioinformatics *27*, 137–139.

71. Ruiz-Carrasco, K., Antognoni, F., Coulibaly, A.K., Lizardi, S., Covarrubias, A., Martínez, E.A., Molina-Montenegro, M.A., Biondi, S., and Zurita-Silva, A. (2011). Variation in salinity tolerance of four lowland genotypes of quinoa (*Chenopodium quinoa* Willd.) as assessed by growth, physiological traits, and sodium transporter gene expression. Plant Physiol. Biochem. *49*, 1333–1341.

72. Nørholm, M.H. (2010). A mutant Pfu DNA polymerase designed for advanced uracil-excision DNA engineering. BMC Biotechnol. *10*, 21.

73. Tzfira, T., Tian, G.W., Lacroix, B., Vyas, S., Li, J., Leitner-Dagan, Y., Krichevsky, A., Taylor, T., Vainstein, A., and Citovsky, V. (2005). pSAT vectors: a modular series of plasmids for autofluorescent protein tagging and expression of multiple genes in plants. Plant Mol. Biol. *57*, 503–516.

74. Sheen, J. (2002). A transient expression assay using *Arabidopsis* mesophyll protoplasts. http://genetics.mgh.harvard.edu/sheenweb/.

75. Costa, A., Gutla, P.V., Boccaccio, A., Scholz-Starke, J., Festa, M., Basso, B., Zanardi, I., Pusch, M., Schiavo, F.L., Gambale, F., and Carpaneto, A. (2012). The *Arabidopsis* central vacuole as an expression system for intracellular transporters: functional characterization of the Cl⁻/H⁺ exchanger CLC-7. J. Physiol. *590*, 3421–3430.

76. Boccaccio, A., Scholz-Starke, J., Hamamoto, S., Larisch, N., Festa, M., Gutla, P.V., Costa, A., Dietrich, P., Uozumi, N., and Carpaneto, A. (2014). The phosphoinositide PI(3,5)P₂ mediates activation of mammalian but not plant TPC proteins: functional expression of endolysosomal channels in yeast and plant cells. Cell. Mol. Life Sci. *71*, 4275–4283.

77. Stigloher, C., Zhan, H., Zhen, M., Richmond, J., and Bessereau, J.L. (2011). The presynaptic dense projection of the *Caenorhabditis elegans* cholinergic neuromuscular junction localizes synaptic vesicles at the active zone through SYD-2/liprin and UNC-10/RIM-dependent interactions. J. Neurosci. *31*, 4388–4396.

78. Reynolds, E.S. (1963). The use of lead citrate at high pH as an electron-opaque stain in electron microscopy. J. Cell Biol. *17*, 208–212.

79. Sack, L., Chatelet, D.S., and Scoffoni, C. (2013). Estimating the mesophyll surface area per leaf area from leaf cell and tissue dimensions measured from transverse cross sections. http://prometheuswiki.org/tiki-index.php?page=Estimating+the+mesophyll+surface+area+per+leaf+area+from+leaf+cell+and+tissue+dimensions+measured+from+transverse+cross-sections.

80. Böhm, J., Scherzer, S., Krol, E., Kreuzer, I., von Meyer, K., Lorey, C., Mueller, T.D., Shabala, L., Monte, I., Solano, R., et al. (2016). The Venus flytrap *Dionaea muscipula* counts prey-induced action potentials to induce sodium uptake. Curr. Biol. *26*, 286–295.

81. Geiger, D., Maierhofer, T., Al-Rasheid, K.A., Scherzer, S., Mumm, P., Liese, A., Ache, P., Wellmann, C., Marten, I., Grill, E., et al. (2011). Stomatal closure by fast abscisic acid signaling is mediated by the guard cell anion channel SLAH3 and the receptor RCAR1. Sci. Signal. *4*, ra32.

82. Arif, I., Newman, I.A., and Keenlyside, N. (1995). Proton flux measurements from tissues in buffered solution. Plant Cell Environ. *18*, 1319–1324.

83. Newman, I.A. (2001). Ion transport in roots: measurement of fluxes using ion-selective microelectrodes to characterize transporter function. Plant Cell Environ. *24*, 1–14.

84. Lagostena, L., Festa, M., Pusch, M., and Carpaneto, A. (2017). The human two-pore channel 1 is modulated by cytosolic and luminal calcium. Sci. Rep. *7*, 43900.

85. Kearse, M., Moir, R., Wilson, A., Stones-Havas, S., Cheung, M., Sturrock, S., Buxton, S., Cooper, A., Markowitz, S., Duran, C., et al. (2012). Geneious Basic: an integrated and extendable desktop software platform for the organization and analysis of sequence data. Bioinformatics *28*, 1647–1649.

STAR★METHODS

KEY RESOURCES TABLE

REAGENT or RESOURCE	SOURCE	IDENTIFIER
Bacterial and Virus Strains		
XL1-Blue MRF' *E. coli* Strain used for cloning	Widely distributed	N/A
Biological Samples		
Chenopodium quinoa cultivar KVL52	University of Copenhagen	[8]
Arabidopsis thaliana Col-0	Lehle Seeds USA	WT-02-45-02
Arabidopsis thaliana clc-a mutant	I2BC, Gif Sur Yvette	[29]
Chemicals, Peptides, and Recombinant Proteins		
Advantage 2 Polymerase Mix for amplification	Takara Bio USA (Clontech Laboratories)	Catalog #639201
Gentamicin sulfate salt	Sigma-Aldrich, Merck	Catalog #G1264
Standard chemicals such as salts and buffers for electrophysiological recordings or for molecular biology	Sigma-Aldrich, Merck	N/A
USER-Enzyme for advanced uracil-excision-based cloning and USER fusion technique [60]	New England Biolabs	Catalog #M5505
Fluorescein diacetate	Sigma-Aldrich, Merck	Catalog # F7378
Poly(ethylene glycol) average Mn 4,000, platelets (PEG)	Sigma-Aldrich, Merck	Catalog # 81240
CELLULASE "ONOZUKA" R-10	Yakult Honsha, Tokyo, Japan	N/A
MACEROZYME R-10	Yakult Honsha, Tokyo, Japan	N/A
Critical Commercial Assays		
NucleoSpin RNA Plant Kit	Macherey-Nagel, Germany	Catalog #740949.250
AmpliCap-Max T7 High Yield Message Maker Kit	Cellscript, Madison, WI, USA	Catalog #C-MSC100625
Deposited Data		
RNaseq	*Chenopodium quinoa* cultivar KVL52	BioProject number PRJNA394652 and accession number E-MTAB-6112
CqHAK sequence	*Chenopodium quinoa* cultivar KVL52	Accession#: CCG024117.1/CCG045154.1
CqClC-c sequence	*Chenopodium quinoa* cultivar KVL52	Accession#: CCG018916.1/CCG067813.1
CqHKT1.1 sequence	*Chenopodium quinoa* cultivar KVL52	Accession#: CCG039537.1
CqHKT1.2 sequence	*Chenopodium quinoa* cultivar KVL52	Accession#: CCG066375.1
CqProT sequence	*Chenopodium quinoa* cultivar KVL52	Accession#: TRINITY_DN108018
McHKT1.2 sequence	*Chenopodium quinoa* cultivar KVL52	Accession#: AAK52962.1
CqP5CS2 sequence	*Chenopodium quinoa* cultivar KVL52	Accession#: CCG065773.1/CG028027.2/CCG047200.1
Experimental Models: Organisms/Strains		
Chenopodium quinoa cultivar KVL52	University of Copenhagen	[8]
Arabidopsis thaliana Col-0	Lehle Seeds USA	WT-02-45-02
Arabidopsis thaliana clc-a mutant	I2BC, Gif Sur Yvette	[29]
Oligonucleotides		
For qPCR primers see Table S3	synthesized by TIB Molbiol Berlin, Germany	This paper
For amplification of transporter and channel CDS (coding sequence) see Table S3	synthesized by Sigma-Aldrich, Merck, Germany	This paper

(Continued on next page)

Continued

REAGENT or RESOURCE	SOURCE	IDENTIFIER
Recombinant DNA		
Oocyte expression vector	[60]	pNB1u
Plant expression vector for N-terminal fusions to a fluorophore for localization studies (fluorophores were GFP and mOrange)	[31, 60]	pSATGFPu, pCambia3300mOrangeu, pMDC43
CDS of quinoa channels and transporters thereof were cloned into pNB1u, pSAT or pCambia for electrophysiological analysis or localization studies	This study	N/A
CDS of AtCIPK23 and AtCBL1 thereof were cloned into pNB1u for electrophysiological analysis in *X. leavis* oocytes.	This study; [38]	N/A
Software and Algorithms		
BLAST (database search program)	https://blast.ncbi.nlm.nih.gov/Blast.cgi?CMD=Web&PAGE_TYPE=BlastDocs&DOC_TYPE=Download, https://blast.ncbi.nlm.nih.gov/Blast.cgi?PAGE=Proteins	[61]
Clustal Omega	https://www.ebi.ac.uk/Tools/msa/clustalo/	[62]
Subread (read aligner)	http://subread.sourceforge.net/	N/A
FeatureCounts (counting reads to genomic features)	http://subread.sourceforge.net/	N/A
EdgeR (differential expression analysis)	https://bioconductor.org/packages/release/bioc/html/edgeR.html	N/A
Trinity (*de novo* assembler)	https://github.com/trinityrnaseq/trinityrnaseq/wiki	N/A
AHRD (annotation pipeline)	https://github.com/groupschoof/AHRD	N/A
Mapman (metabolic pathways and biological processes)	https://mapman.gabipd.org/mapman-download	N/A
SUBAcon (subcellular localization)	http://suba3.plantenergy.uwa.edu.au/	N/A
Paintomics (pathway analysis)	http://www.paintomics.org	N/A

CONTACT FOR REAGENT AND RESOURCE SHARING

Further information and requests for resources and reagents should be directed to and will be fulfilled by the Lead Contact, Rainer Hedrich (hedrich@botanik.uni-wuerzburg.de).

EXPERIMENTAL MODEL AND SUBJECT DETAILS

Plant material and growth conditions
C. quinoa (cv.5020) plants were cultivated in a climate chamber (12 hr daylight, 50% RH, 20°C) using common potting soil. NaCl-treatment was started after 4 weeks of growth. The NaCl concentration in the irrigation water was increased stepwise up to 200 mM. After 5 weeks of salt treatment plant tissue was harvested for RNA extraction. *Arabidopsis thaliana Col-0* wild-type and *Arabidopsis thaliana clca-2* plants [29] were grown on soil in a growth chamber at 22°C and 8 hr light / 16 hr dark regime.

Xenopus oocyte preparation
Investigations on quinoa channels and transporters were performed in oocytes of the African clawfrog *Xenopus laevis*. Permission for keeping *Xenopus* exists at the Julius-von-Sachs Institute and is registered at the government of Lower Franconia (reference number 70/14). Mature female *Xenopus laevis* frogs were kept at 20°C at a 12/12 hr day/night cycle in dark gray 96 l tanks (5 frogs/tank). Frogs were fed twice a week with floating trout food (Fisch-Fit Mast 45/7 2mm, Interquell, Wehringen, Germany). Tanks are equipped with 30 cm long PVC pipes with a diameter of around 10 cm. These pipes are used as hiding places for the frogs. The water is continuously circulated and filtered by a small aquarium pump. For oocyte isolation, mature female *X. laevis* frogs were anesthetized by immersion in water containing 0.1% 3-aminobenzoic acid ethyl ester. Following partial ovariectomy, stage V or VI oocytes were treated with 0.14 mg/mL collagenase I in Ca^{2+}-free ND96 buffer (10 mM HEPES pH 7.4, 96 mM NaCl, 2 mM KCl, 1 mM $MgCl_2$,) for 1.5 hr. Subsequently, oocytes were washed with Ca^{2+}-free ND96 buffer and kept at 16°C in ND96 solution (10 mM HEPES pH 7.4, 96 mM NaCl, 2 mM KCl, 1 mM $MgCl_2$, 1mM $CaCl_2$) containing 50 mg/L gentamycin [63]. For oocyte electrophysiological experiments 10 ng of each

cRNA was injected, except for 25 ng of CqHAK-like cRNA, into selected oocytes. Oocytes were incubated for 2 to 5 days at 16°C in ND96 solution containing gentamycin.

METHOD DETAILS

RNA extraction

RNA was isolated from four biological replicates for each condition. RNA from leaves as well as leaves without bladders was isolated using the E.Z.N.A plant RNA kit (OMEGA Bio-tek) following the manufacturer's instructions. RNA from salt bladders was isolated using the NucleoSpin RNA Plant Kit (Macherey-Nagel) according to the manual with some exceptions. Therefore, young leaves with mostly intact, turgescent bladders were frozen in liquid nitrogen and bladders were brushed off with a small spatula. For each biological replicate bladders of six young leaves from two plants were collected in 500 μL lysis buffer RA1 (containing 1:100 TCEP) and mixed strongly for 20 s to lyse the cells. The lysate was transferred to the NucleoSpin Filters and centrifuged for 1 min at 11,000 g. The filtrate was mixed with 500 μL 70% ethanol and transferred in two steps to the NucleoSpin RNA plant Column and centrifuged for 1 min at 11,000 g. The washing steps were performed following the manufacturer's instructions. RNA was eluted in 33 μL RNase free water that was incubated on the membrane twice for 1 min. Quality control measurements were performed on an Experion automated electrophoresis station (Bio-Rad Hercules, California, U.S.A.) and the concentration was determined using a Nanodrop ND-1000 spectrophotometer (Thermo Fisher Scientific, Wilmington, DE, U.S.A.).

RNA-sequencing and data analysis

To investigate salt-induced changes in the expression patterns of EBCs, we harvested whole leaves from control plants grown without (L) and with salt (L+). Bladder samples were mechanically isolated from leaves by gentle brushing (denoted as B/B+, respectively). The remaining stripped leaves were also sampled (LS/LS+).

The mRNA-seq library was prepared using the NEBNext Ultra Directional RNA Library Prep Kit for Illumina (New England Biolabs) following the manufacturer's standard protocol. Briefly the mRNA was enriched from 1 μg of total RNA using polyT magnetic beads, fragmented by divalent ions and subjected to first strand cDNA synthesis using random primers. Second strand cDNA synthesis was performed by replacing dT with U in the reaction. After end repair, dA-tailing and adaptor ligation, the second strand cDNA and part of the adaptor was removed using the USER enzyme, leaving adaptor-ligated first strand cDNA for PCR amplification. Before sequencing, the quality of libraries was examined on a Fragment Analyzer (Advanced Analytical Technologies, Inc) and the quantity measured using Qubit (Thermo Fisher Scientific) and qPCR. The sequencing was performed on a HiSeq2500 using the SBS v4 reagent at the Core Facility for Genomics of the Shanghai Center for Plant Stress Biology.

The reads were mapped to the quinoa reference genome [4] using the subread tool with default parameters [64]. Detection of the readcounts was performed by the software featureCount with transcript as feature type [65]. The R package edgeR [66] was used for filtering low expressed genes by a cutoff of 0.1 cpm in at least three replicates. The RNaseq data mapped to 40,907 of 54,682 quinoa transcripts representing 75% of the genome. The LRT (likelihood-ratio test) and the treat methods were used to identify differentially expressed genes (DEGs) based on a false discovery rate (FDR) of < 0.05 and of either no fold change (FC) cutoff (LRT) or a log2FC > 2 cutoff (treat) between different genotypes. The high throughput sequencing data for epidermal bladder cell transcriptome analyses are available at the Sequence Read Archive (https://www.ncbi.nlm.nih.gov/sra) under the BioProject number PRJNA394652.

Analyzed comparisons were bladder cells against leaves (B/L), bladder cells against stripped leaves (B/LS), leaves against stripped leaves (L/LS), salt treated bladders against bladders (B+/B), salt treated leaves against leaves (L+/L), salt treated bladders against salt treated leaves (B+/L+), salt treated bladders against salt treated stripped leaves (B+/LS+) and salt treated leaves against salt treated stripped leaves (L+/LS+). Next to this dataset, we additionally generated high coverage RNaseq data of untreated EBC and leaf cells to perform a *de novo* transcriptome assembly applying the TRINITY pipeline [67]. The *de novo* transcripts were annotated by the AHRD pipeline (https://github.com/groupschoof/AHRD) and surveyed for selected genes and gene families of interest to complement the current annotation release and detect missing candidates. RNaseq data have been deposited in the ArrayExpress database at EMBL-EBI (http://www.ebi.ac.uk/arrayexpress) under accession number E-MTAB-6112.

Arabidopsis Gene Identifiers (AGIs) were assigned to 35,664 quinoa transcripts by BLAST [61] search for best-hit. For downstream analysis, AGIs were annotated with MapMan BINs and description lines [68]. To identify the subcellular localization, the tool SubaCon (a subcellular localization database for *Arabidopsis* proteins) (http://suba3.plantenergy.uwa.edu.au/) [69] was used. The pathway analysis was performed by the online tool PaintOmics [70].

cDNA preparation and expression analyses

cDNA was prepared using 2 μg of total RNA after DNA contamination was removed by RNase free DNase I (Thermo Scientific, Waltham MA) digestion in the presence of RiboLock RNase Inhibitor (Thermo Scientific, Waltham MA) following the manufacturers specifications. RNA was precipitated with 5 M NH₄Cl in isopropanol and washed with 70% ethanol. The RNA pellet was resuspended in diethyl pyrocarbonate (DEPC)-treated H₂O and first strand cDNA was synthesized using the M-MLV RT RNase (H-) point mutant (Promega, Mannheim, Germany) following the manufacturers specifications. qPCR was performed using a Realplex Mastercycler system (Thermo Scientific, Waltham MA) and ABsolute QPCR SYBR green capillary mix (Thermo Scientific, Waltham MA) with a final volume of 20 μL containing 2 μL cDNA (1:20 diluted in HPLC water). Gene-specific primer (TIB MOLBIOL, Germany) were designed to amplify small fragments not exceeding 500 bp according to RNaseq sequences and validated prior to qPCR. The expression levels of

each gene were determined by using standards of known concentrations for each primer pair (Table S3) and normalized to 10,000 transcripts of the housekeeping gene, the growth elongation factor EF1α [71].

Cloning and cRNA synthesis

To identify the coding sequence of CqProT (TRINITY_DN108018), CqHAKs (CCG024117.1, CCG045154.1), CqHKT1.1 (CCG039537.1), CqHKT1.2 (CCG066375.1) and CqClC-c (CCG018916.1/CCG067813.1) we used the analyzed RNAseq dataset. Using gene-specific oligonucleotide primers (Table S3), which comprised the CDS (coding sequence) of CqProT, CqHAK-like transporters, CqHKT1-like channels or CqClC-c, and Advantage cDNA Polymerase Mix (Takara Bio USA, Inc) revealed for each gene a sequence identical to the expected from the RNAseq dataset. For heterologous expression in *Xenopus* oocytes, the generated cDNAs of the transport proteins were cloned into oocyte expression vectors (based on pNBIu vectors, see Key Resources Table) by an advanced uracil excision-based cloning technique described by Nour-Eldin et al. [60]. Therefore, the before mentioned PCR products were used as template for USER PCR to attach USER-specific 5'- and 3'-overhangs. PCR conditions were as described by Nørholm et al., 2010 [72] using PfuX7 polymerase. The resulting PCR products of the respective channels, transporters and kinases were treated with the USER enzyme (New England Biolabs, Ipswich, MA, USA) to remove the uracil residues, generating single-stranded overlapping ends. Following uracil excision, recirculation of the plasmid was performed at 37°C for 30 min followed by 30 min at room temperature, and then constructs were immediately transformed into chemical competent *Escherichia coli* cells (XL1-Blue MRF'). All constructs were verified by sequencing. For functional analysis, cRNAs were prepared using the AmpliCap-Max T7 High Yield Message Maker Kit (Cellscript, Madison, WI, USA) by following the manufacturer's instructions. Oocyte preparation and cRNA injection have been described in Experimental Model and Subject Details.

For transient protoplast expression of CqClC-c, the cDNA was cloned into the plant expression vector pSAT [73] (35S promotor and terminator) via the advanced uracil excision-based cloning technique [60]. Thereby CqClC-c was fused N-terminal to the vector-based GFP for localization studies. mOrange:CqHAK, mOrange:CqProT, mOrange:CqHKT1.1 and mOrange:CqHKT1.2 fusion constructs were cloned via the USER-technique into a modified pCAMBIA3300 binary vector containing a pUBQ10 promoter [60].

Protoplast isolation and transformation

Mesophyll protoplasts were isolated from 4-6-week-old *Arabidopsis thaliana* Col-0 or *Arabidopsis thaliana clca-2* mutant plants and 8-9-week-old *Chenopodium quinoa* plants. The lower epidermis of leaves was gently scrubbed with sand paper before incubating them for 3 hr in dark in the enzyme solution (1%–1.5% cellulase R10, 0.2%–0.4% macerozyme R10, 0.4 M mannitol, 20 mM KCl, 20 mM MES, pH 5.7, 10 mM CaCl$_2$, 5 mM, 0.1% BSA). The enzyme solution containing protoplasts was filtered with a 50 μm nylon mesh with W5 buffer (154 mM NaCl, 125 mM CaCl$_2$, 5 mM KCl, 5 mM glucose, 2 mM MES pH 5.7) and the protoplasts were pelleted carefully at 100 g for 2 min. After removing the supernatant, the isolated protoplasts were incubated on ice for 30 min in W5. Protoplasts will descend and W5 could be replaced by MMG solution (∼500 protoplast per μL; 4 mM MES pH 5.7, 0.4 M mannitol, 15 mM MgCl$_2$) and incubated for 15 min at RT. To 20 μg plasmid DNA 200 μL protoplast solution and 220 μL PEG solution (2 g PEG 4000, 1.5 mL H$_2$O, 1.25 mL Mannitol (0.8M), 0.5 mL CaCl$_2$ (1 M)) were added and incubated for 15 min at RT. After adding 1,320 μL W5 the reaction was centrifuged at 100 g for 1 min. The supernatant was removed, and the protoplasts were kept in 1.5 mL W5 buffer in the dark and at RT for 2 days [74, 75].

For patch clamp analysis of CqClC-c and AtClC-a vacuoles were released from protoplasts by bath perfusion of VR solution [76] containing 100 mM malic acid, 155 mM 1,3-bis(tris(hydroxymethyl)methylamino)propane (BTP), 5 mM ethylene glycol-bis(2-amino-ethylether)-N,N,N′,N′-tetraacetic acid (EGTA), 3 mM MgCl2, pH 7.5, adjusted to 450 mOsm with D-sorbitol.

Electron microscopy

C. quinoa leaves were cut with razor blades to fit into the 3 mm diameter High Pressure Freezing (HPF) Specimen Carriers Type A (200μm, Leica), covered with hexadecene as filler and closed with an HPF Specimen Carriers Type B (0 μm, Leica). Samples were high pressure frozen with an EM HPM 100 (Leica) at > 2100 bar with a freezing speed > 20 000 K/s. Specimen Carrier sandwiches were opened in liquid nitrogen and the vitrified samples were freeze substituted in the AFS2 (Leica) and embedded according to the published protocol [77] with modifications:

Duration	Reagent	Temperature/Ramp
96 hr	0.1% tannic acid, 0.5% glutaraldehyde in anhydrous acetone (exchange with fresh solution at day 2)	−90°C
1 hr	4x washes with anhydrous acetone	−90°C
28 hr	2% OsO$_4$ in anhydrous acetone	−90°C
14 hr	same solution as last step	−90°C to −20°C
16 hr	same solution as last step	−20°C
4 hr	same solution as last step	−20°C to 4°C
2 hr	4x washes with anhydrous acetone	4°C

After gradually raising the temperature to room temperature within 1 hr samples were infiltrated with Epon and polymerized at 60°C for 72 hr. 80 nm sections were cut with a Leica EM UC7, transferred on pioloform coated copper grids (Plano) and contrasted 15 min with 2.5% uranyl acetate in ethanol, washed, again contrasted in Reynolds' lead [78] citrate for 10 min, thoroughly washed and dried. Sections were images on a JEOL JEM-2100 at 200 kV transmission electron microscope with a TemCam F146 (Tietz Video and Imaging Processing Systems) with the EM Menu Software (Tietz Video and Imaging Processing Systems).

Confocal microscopy
Chloroplast fluorescence
For chloroplast fluorescence detection in single bladders, young quinoa leaves were cut into small stripes (cross-sections) and images were taken with a Leica (RM2165) equipped with a Leica HCX PL APO CS 40.0x1.10 WATER UV objective. The same settings were used for the imaging of the chloroplast fluorescence in mesophyll protoplasts. The chlorophyll fluorescence of chloroplasts was observed at an excitation wavelength of 405 nm. Chloroplast fluorescence was detected between 580 and 720 nm. Z stack with 20 steps and a step size of 8 μm.

For chloroplast quantification and fluorescein diacetate (FDA) fluorescence detection in EBCs and mesophyll cells, the cross-sections were immediately floated on basal salt media (0.5 mM KCl, 0.1 mM CaCl$_2$, pH 5.6) containing 5 μg mL^{-1} FDA for 15 min (mesophyll) or 1 hr (bladders). Following incubation in FDA, all stained tissues were washed in BSM for 3 min to remove residual dyes before measuring fluorescence intensity by confocal microscopy. All dying steps were done at room temperature and in darkness. Confocal microscopy was performed with a Zeiss LSM 510 Meta laser scanning confocal microscope equipped with a Plan-Apochromat 20x/0.8 Ph2 objective to visualize bladders cells or a Plan-Apochromat 63x/1.40 Oil DIC objective for mesophyll cells. The fluorescence of FDA and chlorophyll was imaged using a 488 nm laser for excitation and emission collected between 505 and 530 nm (FDA) and 660 and 710 nm (chlorophyll autofluorescence). To capture images of an entire bladder cell, consecutive series of confocal sections were taken in the z direction at 4 μm intervals and chloroplast counted in each section. For the mesophyll cells, total number of chloroplasts was estimated based on chloroplasts counted from planar and longitudinal sections of the palisade mesophyll cells. The percentage of the cell occupied by the cytosol was estimated by measuring the area stained with FDA. For the mesophyll, the volume of the cell and vacuole was estimated based on the method in [79].

Localization studies
Measurements were performed on a Leica SP5 confocal laser scanning microscope (Leica Microsystems CMS, Mannheim, Germany) and the water immersion objective lens Leica HCX IRAPO L25 × /0.95W was used for imaging Arabidopsis mesophyll pro-toplasts for confocal imaging. mOrange fusion proteins were excited with a 562 nm diode laser and mOrange fluorescence emission was detected between 560 and 620 nm. Chlorophyll autofluorescence was detected at 630 to 750 nm.

Oocyte recordings
Functional characterization of transport proteins was performed in oocytes of the African clawfrog Xenopus laevis at RT.
Two-electrode voltage-clamp
In two-electrode voltage-clamp (TEVC) studies, oocytes were perfused with citric acid/Tris-based (pH 4) or MES/Tris-based (pH $\geq$ 5.5) buffers. The standard bath solution contained 10 mM citric acid/Tris or 10 mM MES/Tris and 1 mM CaCl$_2$, 1 mM MgCl$_2$ and 1 mM LaCl$_3$. The osmolality of each solution was adjusted to 220 mOsm/kg using D-sorbitol. For the cation transport proteins the ionic strength for measurements under varying substrate concentrations was balanced with lithium for a total concentration of 100 mM. For current-voltage relations (IV curves), single-voltage pulses were applied in 10 mV decrements from +60 to −200 mV starting from a holding potential of 0 mV. Deviations of this standard pulse protocol are mentioned in the figure legends [24, 38, 80, 81]. To determine the K$_m$ value of CqHAK and CqHKT1.1 for potassium or sodium, respectively, the currents were normalized to the highest applied cation concentration at −120 mV. The resulting dose-response curve was described by the Michaelis-Menten Equation 1:

$$f(x) = (I_{max} * x)/(K_m + x)$$ (Equation 1)

To estimate the relative open probability of CqHKT1.2 channels instantaneous currents (I$_{inst}$) were extracted immediately after the voltage jump from the test pulses to the holding potential. For the calculation of the relative open probability the following Boltzmann Equation 2 was used:

$$Po = offest + 1/(1 + \exp(V_{!/2} - V_m)/z)$$ (Equation 2)

where V$_{1/2}$ is the half maximal activation voltage, V$_m$ is the membrane potential and z is the slope of the Boltzmann function. The currents were normalized to the saturation value of the calculated Boltzmann distribution.
Ion flux measurements
Ion flux measurements were performed additionally on TEVC voltage-clamped oocytes. The ion fluxes over the oocyte plasma membrane (PM) were monitored using non-invasive ion-selective scanning microelectrodes. To avoid artificial flux measurements e. g. caused by a PM-rupture at the impalement site of the TEVC electrodes, both techniques were performed at opposite sides of the oocyte. The standard bath solution for combined TEVC and ion flux measurements contained 2 mM KCl and 0.2 mM citric acid/Tris (pH 4) for CqHAK5 measurements and 10 mM NaCl and 0.2 mM MES/Tris (pH 5.6) for CqHKT1.1 and 1.2 measurements.

Osmolality of each solution was adjusted to 220 mOsm/kg using myo-Inositol. The ion-selective electrodes were pulled from boro-silicate glass capillaries w/o filament (Ø 1.0 mm, Science Products) with a vertical puller (Narishige Scientific Instrument Lab). They were baked over night at 220°C and silanized with N, N-Dimethyltrimethylsilylamine (Sigma-Aldrich) for 1 hr. K+-and Na+-selective electrodes were backfilled with 100 mM of the respective ion and the tip was filled with potassium ionophore I cocktail A or sodium ionophore I cocktail A (Sigma-Aldrich). Calibration of selective electrodes was performed at 0.2, 2 and 20 mM KCl and 0.5, 5 and 50 mM NaCl, respectively. Only electrodes that recorded a shift in voltage of around 59 mV per 10x change in K+/Na+ concentration were used. The ion-selective electrodes were positioned with a SM-17 Micromanipulator (Narishige Scientific Instrument Lab) at ap-prox. 5 μm distance to the oocyte equator using an upright microscope (Axioskop, Carl Zeiss AG). The electrodes were connected via Ag/AgCl half-cells to head stages (Applicable Electronics, USA) of an Ion/ Polarographic Amplifier (Applicable Electronics, USA). Electrodes scanned the oocyte at 10 s intervals between two positions with a distance of 100 μm, using a micro-stepping motor driver (US Digital, USA). Raw data were acquired with a NI USB 6259 interface (National Instruments), using custom-built Labview-based software "Ion Flux Monitor." Raw voltage data were converted offline into ion flux data, as described previously [82, 83]. In brief, mean values of the voltages measured with ion-selective electrodes at both positions were calculated and the voltage difference dV between both positions was computed and inserted in Equation 3. The Flux J was calculated using equation:

$$J = cuF(58/Nernst\ slope)(dV/dx) \tag{Equation 3}$$

With the following parameters; the ion concentration c (mol m^{-3}), the mobility of the ion u (m^2 s^{-1} volt^{-1}), the Nernst slope originating from the calibration, the voltage difference dV (volt) between both positions, and the distance between both positions dx (m). In case of the spherical oocyte the distance was corrected using:

$$dx = r^2[1/(r+x) - 1/(r+x+dx_1)] \tag{Equation 4}$$

With r being the radius of the oocyte, x the minimum distance to the oocyte and dx_1 as the distance between both positions (100 μm in our case).

Patch-clamp recordings

Patch-clamp experiments on GFP-positive vacuoles were performed in the whole-vacuole configuration at RT, as described else-where [84], using an EPC-7 patch clamp amplifier (HEKA Elektronik, Lambrecht, Germany). Patch pipettes were pulled from thin-walled borosilicate glass (Clark Electrochemical Instruments, Pangbourne, Reading, UK), with a tip resistance of 3 - 3.5 MOhm. The pipette solution contained (in mM): 100 KCl, 3 MgCl$_2$, 20 MES, adjusted to pH 5.5 (with KOH) and 480 mOsm (with D-sorbitol). Bath solutions contained (in mM): 100 K-x, 2 EGTA, 3 MgSO$_4$, 10 HEPES, adjusted to pH 7.2 (with KOH) and 480 mOsm (with D-sorbitol), where x was either gluconate, chloride or nitrate.

High-resistance membrane seals were generally formed in VR solution. After the establishment of the whole-vacuole configuration, the bath solution was exchanged, and membrane currents were allowed to stabilize for 10-15 min. Bath solutions were exchanged by means of a gravity-driven perfusion system coupled to a peristaltic pump.

Membrane currents were elicited by 1 s voltage steps ranging from +80 to –80 mV in 20 mV decrements, followed a 500 ms voltage step to +50 mV. The holding potential was set to 0 mV.

Positive currents correspond to anions flowing from the lumen of the vacuole to the cytoplasmic side or to cations moving in the opposite direction.

Alignment and phylogenetic analysis of CqHKTs

Selected HKT orthologs were identified by BLASTP and the corresponding accession numbers are listed in Data and Software Availability section. The amino acid sequences were aligned with Clustal Omega [62]. The phylogenetic relation between HKT proteins was performed with the software Geneious R9 [85] using the Neighbor-Joining method.

QUANTIFICATION AND STATISTICAL ANALYSIS

All results were gained from $\geq$ two independent experiments. Results are given as mean ± standard deviation (SD) or standard error (SE) as indicated in the figure legend. For statistical analysis and graph preparations the software Igor Pro7 (WaveMetrics, Lake Oswego, Oregon, USA) and Excel (Microsoft, Redmond, Washington, USA) was used.

DATA AND SOFTWARE AVAILABILITY

The high throughput sequencing data for epidermal bladder cell transcriptome analyses are available at the Sequence Read Archive (https://www.ncbi.nlm.nih.gov/sra) under the BioProject number PRJNA394652 [4]. RNaseq data of untreated EBC and leaf cells for a *de novo* transcriptome have been deposited in the ArrayExpress database at EMBL-EBI (http://www.ebi.ac.uk/arrayexpress) under accession number E-MTAB-6112.

The identifiers of the characterized proteins of quinoa are: CqHAK (CCG024117.1/CCG045154.1), CqClC-c (CCG018916.1/CCG067813.1), CqHKT1.1 (CCG039537.1), CqHKT1.2 (CCG066375.1), CqProT (TRINITY_DN108018), CqP5CS2 (CG028027.2/CCG047200.1). Furthermore, the identifiers are mentioned in Method Details and Key Resources Table. The accession number and plant species, which were used for phylogenetic relation analyses of HKT transport proteins, are listed below:

Oryza sativa: OsHKT1;1 (CAD37183.1), OsHKT1;3 (CAD37185.1), OsHKT1;4 (CAD37197.1), OsHKT1;5 (BAB93392.1), OsHKT2;1 (BAB61789.1), OsHKT2;2 (BAB61791.1), OsHKT2;3 (CAD37187.1), OsHKT2;4 (CAD37199.1). *Triticum aestivum*: TaHKT2;1 (AAA52749.1). *Hordeum vulgare*: HvHKT2;1 (CAJ01326.1). *Phragmites australis*: PaHKT2;1 (BAE44385.1). *Suaeda salsa*: SmHKT1;1 (AAS20529.2). Eucalyptus camaldulensis: EcHKT1;1 (AAF97728.1), EcHKT1;2 (AAD53890.1). *Mesembryanthemum crystallinum*: McHKT1.1 (AAO73474.1), McHKT1.2 (AAK52962.1). *Arabidopsis thaliana*: AtHKT1;1 (AAF68393.1). *Dionaea muscipula*: DmHKT1 (ALO61068.1). *Eutrema salsugineum*: TsHKT1;2 (AFJ23835.1). *Beta vulgaris*: BvHKT1;1 (XP_010690257.1), BvHKT1;2 (XP_010690256.1), BvHKT1;3 (XP_010688439.1).

Software and algorithms used in this study are listed in the Key Resources Table. In addition, for graph preparations and statistical analysis the software Igor Pro7 (WaveMetrics, Lake Oswego, Oregon, USA), Excel (Microsoft, Redmond, Washington, USA), and CorelDRAW (Corel Corporation, Ottawa, Ontario, Canada) and for electron microscopy the EM Menu Software (Tietz Video and Imaging Processing Systems) was used.